

Anoxic and Oxidic Oxidation of Rocks Containing Fe(II)Mg-Silicates and Fe(II)-Monosulfides as Source of Fe(III)-Minerals and Hydrogen. Geobiotropy.

Marie-Paule Bassez¹

Received: 11 July 2016 / Accepted: 2 March 2017 /
Published online: 31 March 2017

© Springer Science+Business Media Dordrecht 2017

Abstract In this article, anoxic and oxidic hydrolyses of rocks containing Fe (II) Mg-silicates and Fe (II)-monosulfides are analyzed at 25 °C and 250–350 °C. A table of the products is drawn. It is shown that magnetite and hydrogen can be produced during low-temperature (25 °C) anoxic hydrolysis/oxidation of ferrous silicates and during high-temperature (250 °C) anoxic hydrolysis/oxidation of ferrous monosulfides. The high-T (350 °C) anoxic hydrolysis of ferrous silicates leads mainly to ferric oxides/hydroxides such as the hydroxide ferric trihydroxide, the oxide hydroxide goethite/lepidocrocite and the oxide hematite, and to Fe(III)-phyllosilicates. Magnetite is not a primary product. While the low-T (25 °C) anoxic hydrolysis of ferrous monosulfides leads to pyrite. Thermodynamic functions are calculated for elementary reactions of hydrolysis and carbonation of olivine and pyroxene and E-pH diagrams are analyzed. It is shown that the hydrolysis of the iron endmember is endothermic and can proceed within the exothermic hydrolysis of the magnesium endmember and also within the exothermic reactions of carbonations. The distinction between three products of the iron hydrolysis, magnetite, goethite and hematite is determined with E-pH diagrams. The hydrolysis/oxidation of the sulfides mackinawite/troilite/pyrrhotite is highly endothermic but can proceed within the heat produced by the exothermic hydrolyses and carbonations of ferromagnesian silicates and also by other sources such as magma, hydrothermal sources, impacts. These theoretical results are confirmed by the products observed in several related laboratory experiments. The case of radiolyzed water is studied. It is shown that magnetite and ferric oxides/hydroxides such as ferric trihydroxide, goethite/lepidocrocite and hematite are formed in oxidic hydrolysis of ferromagnesian silicates at 25 °C and 350 °C. Oxidic oxidation of ferrous monosulfides at 25 °C leads mainly to pyrite and ferric oxides/hydroxides such as ferric trihydroxide, goethite/lepidocrocite and hematite and also to sulfates, and at 250 °C mainly to magnetite instead of pyrite, associated to the same ferric oxides/hydroxides and sulfates. Some examples of geological terrains, such as Mawrth Vallis on Mars, the Tagish

✉ Marie-Paule Bassez
mpbassez@hotmail.com; marie-paule.bassez@unistra.fr

¹ Institut de Technologie, Université de Strasbourg, 72 route du Rhin, 67400 Illkirch, France

Lake meteorite and hydrothermal venting fields, where hydrolysis/oxidation of ferromagnesian silicates and iron(II)-monosulfides may occur, are discussed. Considering the evolution of rocks during their interaction with water, in the absence of oxygen and in radiolyzed water, with hydrothermal release of H₂ and the plausible associated formation of components of life, geobiotropic signatures are proposed. They are mainly Fe(III)-phyllosilicates, magnetite, ferric trihydroxide, goethite/lepidocrocite, hematite, but not pyrite.

Keywords Physical-chemistry · Geochemistry · Exobiology · Astrobiology · Origin of life · Prebiotic chemistry

Introduction

In this article, we attempt to propose geological minerals which may be associated with the formation of molecular components of life. Considering that synthesis of molecules of biological interest may be a consequence of the evolution of rocks in their alteration with water, we search for signatures inside rocks which can witness plausible prebiotic synthesis. This work refers to the laboratory experiments on amino acid synthesis when CO/CO₂ and N₂ and an excitation source are present. It has been demonstrated that peptide like molecules are formed when 350 Torr CO and 350 Torr N₂ gases are present above liquid water producing 20 Torr H₂O, and when this gas mixture is excited with high energy particles and photons simulating cosmic radiation: 2.5 to 4.0 MeV protons generated by a van de Graaf accelerator, 40 MeV protons and 65 MeV helium ion beams from an SF cyclotron, 400 MeV and 1 GeV electron beams from an electron synchrotron (Kobayashi et al. 1998), heavy ions (helium, carbon, neon and argon) from an HIMAC heavy ions accelerator, UV light and soft-X rays of keV-order in energy from a synchrotron, and gamma rays of MeV-order from a ⁶⁰Co source (Kobayashi et al. 2008). In these experiments, amino acids precursors are formed with particles, gamma rays and X-rays, not with UV light. Amino acids are detected in small amounts when vacuum UV irradiates NH₃ instead of N₂. For irradiation by protons, helium ions and electrons, the glycine energetic yield, the G-value, which is the amount of molecules formed per 100 eV absorbed, is in proportion to the total energy deposited, and is independent of the kind of particles. The G-value for gamma rays of low-dose rate (<5 Gy/h) is equivalent to the one obtained with 3 MeV protons and is lower for high-dose rates (>90 Gy/h).

It has been demonstrated that CO and not CO₂ is the necessary molecule in the synthesis of amino acids. Indeed, when mixtures of CO, CO₂, N₂, and H₂O are irradiated, the yield of amino acids is clearly connected to the partial pressure of CO (Kobayashi et al. 1990). Many attempts had been carried out earlier to synthesize organic compounds from CO and CO₂ (ref herein Schlesinger and Miller 1983) and the observation that CO was more necessary than CO₂ was suggested in experiments on prebiotic synthesis using spark discharge and conducted for the comparison of primitive atmospheres containing CH₄, CO and CO₂ (Schlesinger and Miller 1983), where it is shown that "*for a H₂/CO₂ ratio of 0, the yield of amino acids is extremely low (5x10⁻³% with added NH₃)*" and "*the amino acid yields at H₂/CO=0 are 0.44% with added NH₃*". Several experiments conducted in liquid and gas phases show conditions of formation of CO. For example, dissolved CO associated with minor dissolved CH₄ is proved experimentally to be a product of the hydrothermal reaction of H₂ on CO₂ dissolved in sea water at 250 °C–300 °C and 250 bars and with addition of Fe₃O₄ as catalyst (Fu and Seyfried 2009). CO gas is also a product of the hydrogenation at atmospheric pressure, of CO₂ gas by a

flux of H_2 at 500 °C and with Cu/Al_2O_3 as catalyst (Chen et al. 2000). CO can thus form in the gas and dissolved states, from high temperature hydrogenation of CO_2 .

Images of the macromolecules which are abiotically formed during a 3 MeV-proton excitation of the ($CO + N_2 + H_2O$) gas mixture has been studied by three-dimensional Scanning Electron Microscopy, 3D-SEM, and 3D Atomic Force Microscopy, 3D-AFM (Bassez et al. 2012). They show nano- and micro-structures of spheres, filaments and tubules, to be compared with morphologies attributed to microorganisms. A wide variety of amino acids were detected after HCl acid-hydrolysis: glycine, D,L-alanine, D,L- α -aminobutyric acid, D,L-aspartic acid, β -alanine, D,L-serine and others and an enantiomer analysis showed a racemic mixture of the most abundant chiral amino acid D, L-alanine thus excluding potential contamination in this abiotic synthesis.

Consequently prebiotic molecules of biological interest can form in media enabling hydrothermal concentration of H_2 , CO_2 and N_2 in the presence of gaseous water and submitted to energetic excitation sources but not UV light.

In the present work, two kinds of rocks are considered in their release of H_2 , ferromagnesian silicate rocks and ferrous monosulfide rocks. Their interaction with water which is oxygenated or not, is studied using thermodynamic functions and thermodynamic E-pH diagrams. The results of the calculations and analyses show that H_2 can be released during the anoxic hydrolysis of the ferromagnesian silicates and ferrous monosulfides, depending on pH and temperature. They show that magnetite may not be a product of the high-T (350 °C) anoxic hydrolysis of the ferromagnesian silicates at pH above ~11.5 but may be a product of their low-T hydrolysis at pH ~8.5. Magnetite seems to be a product of the anoxic hydrothermal hydrolysis of ferrous monosulfides at 250 °C and low pH ~3.5 to 8. This endothermic reaction may occur in symbiosis with the exothermic hydrolyses and carbonations of ferromagnesian silicates rocks and probably also within the heat produced by meteorite/asteroid impacts, magma and hydrothermal sources. Instead at 25 °C, the anoxic hydrolysis of ferrous monosulfides leads to pyrite at pH ~5.4 to 9.5. These theoretical results are related to the process of serpentinization for which a recent article describes a thorough context of the past (Klein et al. 2015 and ref. herein). The serpentinization reaction is usually written with production of serpentine, brucite, magnetite, and H_2 . Our results show that high-T (350 °C) serpentinization do not produce magnetite but rather Fe(III)-phyllosilicates, ferric trihydroxides, goethite/lepidocrocite, hematite and H_2 at high pH above ~11.5, and that it is low-T serpentinization which may produce magnetite around pH 8.5. These theoretical results are confirmed by laboratory experiments. For instance, an experiment conducted on grounded pieces of peridotite, 50 to 100 μm in size, "defined as spinel lherzolite" and "composed of 62 vol% olivine, 26 vol% orthopyroxene, 10 vol% clinopyroxene, ~2 vol% spinel", reacting with seafloor water at 200 °C and 500 bar during 3 to 7 months, showed that "surprisingly magnetite was only present in trace amounts" (Seyfried et al. 2007). Artificial seawater was prepared with chloride, sulfate and bicarbonate. Value of pH measured at 25 °C started at 6.2 and reached a stable value of 12.1 after 3705 h (~5 months). Dissolved H_2 reached the high concentration of 57.4 $mmol.kg^{-1}$ after 3705 h and 76.4 $mmol.kg^{-1}$ after 5187 h (~7 months). Another experiment reports the reaction of cm-sized pieces of uncrushed harzburgite-peridotite with chemically modified seawater at 300 °C and 35 MPa for ca. 1.5 years. Serpentine is formed with accessory magnetite, chlorite, traces of calcite and heazlewoodite. (Klein et al. 2015). "The peridotite can be classified as a harzburgite consisting of olivine (~70 wt%), orthopyroxene (~25 wt%), clinopyroxene (~4 wt%), Cr-spinel (~0.9 wt%) and traces (<0.1 wt%) of amphibole, glass, and primary sulfides...The pH (25°C) increased from 6.3 to 9.0 ... The concentration of $H_{2(aq)}$ increased to 7.7 $mmol/kg$... Pentlandite is found together with magnetite...when fluid

accessed the sulfides, heazlewoodite and magnetite precipitated." Thus, it seems that magnetite is formed during the hydrothermal hydrolysis of sulfides instead of silicates confirming our theoretical results. Other related experiments conducted on sulfides at 25 °C and 250 °C are discussed. The case of oxidic oxidation is also discussed when H₂ is produced in radiolyzed water at high- and low-T. Thus, signatures of oxidic hydrolysis of silicates and sulfides which could have been associated to prebiotic syntheses are also proposed.

Preliminary results have been reported earlier (Bassez 2013, 2014, 2015, 2016). Thermodynamic equations for the elementary reactions of hydrolyses and carbonations of ferromagnesian silicates are re-examined. Some examples of geological terrains where hydrolysis/oxidation of ferromagnesian silicates and ferrous sulfides may occur, are discussed. I call geobiotropic signatures the geological signs, resulting from the hydrothermal evolution of rocks during their interaction with water, and which may witness prebiotic syntheses. Here are presented the geobiotropic signs which can be produced in geological terrains, in symbiosis with the prebiotic syntheses based on Kobayashi experiments.

Calculation Methods

Calculations are performed with the purpose to obtain values of the thermodynamic functions enthalpies and free enthalpies. Elementary reactions are considered for the hydrolysis and carbonation of olivine and pyroxene and for the dehydration of the serpentine group chrysotile/lizardite. They are independent of the chemical composition of olivine and pyroxene. Thermodynamic functions are calculated for the serpentinization process of olivine with the chemical composition (Fe_{0.5}Mg_{0.5})₂SiO₄ and of pyroxene as (Fe_{0.5}Mg_{0.5})SiO₃ and considering the same molar amount of endmember for the hydrolysis and carbonation, 1/4 Fe₂SiO₄ and 1/4MgSiO₃. Units are given per mole of advancement of the reactions. Individual values for reactants and products are taken from Robie and Hemingway's 1995 tables, at 298.15 K and 1 bar (Robie and Hemingway 1995). Values for SiO₂ are those of quartz and for Mg₃Si₂O₅(OH)₄ those of the serpentine chrysotile. Entropy values for (1) and (5) are calculated considering S⁰(H₂) = 130.45 J.K⁻¹.mol⁻¹. Calculations are performed by hand without any computer software. Values of enthalpies, and free enthalpies also named Gibbs energies, are calculated considering the enthalpies and free enthalpies of formation of the reactants and products, $\Delta_r H^0 = \sum_i \nu_i \cdot \Delta_f H_i^0$ and $\Delta_r G^0 = \sum_i \nu_i \cdot \Delta_f G_i^0$. For verification that results are reliable, values of free enthalpies $\Delta_r G^0$, are also calculated considering that $\Delta_r G^0$ is the enthalpy which remains when the energy corresponding to the entropy has been removed from the enthalpy $\Delta_r H^0$: $\Delta_r H^0 - T \cdot \Delta_r S^0$. (see Bassez 1998–2013 for details on thermodynamics).

Thermodynamic functions give information on the heat produced or absorbed during the reaction. In order to get information on the kind of reactions which may occur as a function of pH, temperature and pressure, thermodynamic equilibrium E-pH diagrams also known as Pourbaix diagrams are analyzed. These E-pH diagrams indicate product stability domains. They are constructed at a specific temperature and for concentrations which are usually 10⁻⁶ mol.kg⁻¹, which might not be the concentration in geological terrains. However they are useful to extract some information, write redox equations and understand which reactions may occur as a function of T, P and pH and other dissolved species. For instance, from the analysis of the diagram constructed for iron and water, in high subcritical and low supercritical water, at 350 °C, 25 MPa at total concentration of dissolved iron 10⁻⁶ mol.kg⁻¹ (Fig.7a of Cook and Olive 2012), I deduced that ferrous iron is transformed into ferric iron with release

of H_2 at high pH ~ 11.5 to 14, and I write the redox eq. (10) of Table 2. The redox potential line of the H^+/H_2 couple is higher than the redox potential line of the Fe^{3+}/Fe^{2+} couple. The H^+/H_2 couple oxidizes the Fe^{3+}/Fe^{2+} couple. Equations satisfying the three equilibria of mass, charge and oxidoreduction can thus be written for specific T, P, pH and concentration. The kinetics of the reactions is not the purpose of the present article.

Results

Anoxic Alteration of Ferromagnesian Silicate and Ferrous Monosulfide Rocks

Ferric Phyllosilicates and Ferric Oxides/Hydroxides with Carbonates as Products of the Hydrothermal Anoxic Alteration of Ferromagnesian Silicate Rocks and Magnetite as Product of the Low-T Alteration

Elementary reactions of the serpentinization process inside ultramafic rocks are studied here thermodynamically. The functions enthalpies and free enthalpies for the hydrolyses of the iron endmembers of olivine and pyroxene are calculated with the products either magnetite or ferric trihydroxide or hematite (eqs. 1,1',1'' and 5,5',5'' of Table 1). They show that the process of hydrolysis is endothermic and non spontaneous. However, these hydrolyses may be induced by six exothermic and spontaneous reactions: the four reactions of carbonation of the two olivine endmembers, fayalite Fe_2SiO_4 and forsterite Mg_2SiO_4 (eq. 3 and 4) and the two pyroxene endmembers, ferrosilite $FeSiO_3$ and enstatite $MgSiO_3$ (eq. 7 and 8), and the two reactions of hydrolysis of the magnesium endmembers of olivine and pyroxene (eq. 2 and 6), as far as the activation energies of these reactions are overcome by a triggering effect. Talc, $Mg_3Si_4O_{10}(OH)_2$, a tetrahedral-octahedral-tetrahedral (T-O-T) phyllosilicate, can form in a silica-saturated hydrothermal fluid, following eq. (9), during the slightly exothermic and spontaneous dehydration of lizardite/chrysotile, $Mg_3Si_2O_5(OH)_4$, tetrahedral-octahedral (T-O) phyllosilicates of the serpentine group. An experiment conducted in 2013 proves the validity of eq. (4). When forsterite was exposed to pure deionized water and supercritical CO_2 at 120 °C and 80 bars over 7 days, crystals of magnesite $MgCO_3$ and spherical particles of quartz SiO_2 , were observed (Aaberg et al. 2013). Which one of these three reactions of hydrolysis really occurs?

Thermodynamic E-pH diagrams can give information. Fig. 7a of Cook and Olive (2012) shows the E-pH diagram for iron in high subcritical and low supercritical water, at 350 °C, 25 MPa, and total concentration of dissolved iron 10^{-6} mol.kg $^{-1}$. The redox eq. (10) of Table 2 can be deduced from this diagram. This equation can be written, considering that the trihydroxide anion $Fe(OH)_3^-$, the dissolved form of ferrous dihydroxide $Fe(OH)_2$, contains iron(II) and the tetrahydroxide anion $Fe(OH)_4^-$, the dissolved form of ferric trihydroxide $Fe(OH)_3$, also named hydrated goethite $\alpha-FeO(OH)H_2O$, contains iron(III). In alkaline water, goethite $\alpha-Fe(III)O(OH)$, dissolves as the species $Fe(OH)_4^-$, which is the anion form of $Fe(OH)_3$ and which can be written as $FeO(OH)H_2O(OH)^-$. It is known that ferric iron speciation is controlled by the species Fe^{3+} , $Fe(OH)_2^+$ and $Fe(OH)_4^-$ depending on pH (Albarède 2003). Thus, at 350 °C and high pH, above ~ 11.5 , there is formation of ferric iron under the form of dissolved goethite, $Fe(OH)_4^-$, with release of H_2 . These pH values and the observation that ferric ions form under the form of goethite instead of magnetite most probably explain the results of the Seyfried experiment on the hydrolysis of peridotite, cited in the introduction, where "surprisingly magnetite was only present in trace amounts" (Seyfried et al. 2007).

Table 1 Enthalpies and free enthalpies of hydrolysis and carbonation of olivine (Fe_{0.5}Mg_{0.5}SiO₄, (1) to (4)), and pyroxene (Fe_{0.5}Mg_{0.5}SiO₃, (5) to (8)), and of dehydration of chrysothile (9)

	$\Delta_f H^0$ kJ/mol = $\sum \nu_i \Delta_f H_i^0$	$\Delta_f G^0$ kJ/mol = $\sum \nu_i \Delta_f G_i^0$	$\Delta_f G^0$ kJ/mol = $\Delta_f H^0 - T \Delta_f S^0$
Hydrolysis and carbonation of olivine (Fe_{0.5}Mg_{0.5})₂SiO_{4(s)}			
1/4 Fe ₂ SiO _{4(s)} + 1/6 H ₂ O _(l) → 1/6 Fe ₃ O _{4(s)} + 1/4 SiO _{2(s)} + 1/6 H _{2(g)}	+3.56	+1.43	+1.43 (1)
1/4 Fe ₂ SiO _{4(s)} + H ₂ O _(l) → 1/2 Fe(OH) _{3(s)} + 1/4 SiO _{2(s)} + 1/4 H _{2(g)}	+3.47	+3.35	+3.34 (1) [*]
1/4 Fe ₂ SiO _{4(s)} + 1/4 H ₂ O _(l) → 1/4 Fe ₂ O _{3(s)} + 1/4 SiO _{2(s)} + 1/4 H _{2(g)}	+6.77	+3.87	+3.85 (1) ^{**}
1/4 Mg ₂ SiO _{4(s)} + 3/8 H ₂ O _(l) → 1/8 Mg ₃ Si ₂ O ₅ (OH) _{4(s)} + 1/8 Mg(OH) _{2(s)}	-10.13	-5.92	(2)
1/4 Fe ₂ SiO _{4(s)} + 1/2 CO _{2(g)} → 1/2 FeCO _{3(s)} + 1/4 SiO _{2(s)}	-39.32	-13.50	(3)
1/4 Mg ₂ SiO _{4(s)} + 1/2 CO _{2(g)} → 1/2 MgCO _{3(s)} + 1/4 SiO _{2(s)}	-44.32	-18.22	(4)
Hydrolysis and carbonation of pyroxene (Fe_{0.5}Mg_{0.5})SiO_{3(s)}			
1/4 FeSiO _{3(s)} + 1/12 H ₂ O _(l) → 1/12 Fe ₃ O _{4(s)} + 3/12 SiO _{2(s)} + 1/12 H _{2(g)}	+1.97	+0.79	+0.80 (5)
1/4 FeSiO _{3(s)} + 1/2 H ₂ O _(l) → 1/4 Fe(OH) _{3(s)} + 1/4 SiO _{2(s)} + 1/8 H _{2(g)}	+1.92	+1.75	+1.74 (5) [*]
1/4 FeSiO _{3(s)} + 1/8 H ₂ O _(l) → 1/8 Fe ₂ O _{3(s)} + 1/4 SiO _{2(s)} + 1/8 H _{2(g)}	+3.57	+2.01	+2.02 (5) ^{**}
1/4 MgSiO _{3(s)} + 1/6 H ₂ O _(l) → 1/12 Mg ₃ Si ₂ O ₅ (OH) _{4(s)} + 1/12 SiO _{2(s)}	-5.19	-3.30	(6)
1/4 FeSiO _{3(s)} + 1/4 CO _{2(g)} → 1/4 FeCO _{3(s)} + 1/4 SiO _{2(s)}	-19.47	-6.67	(7)
1/4 MgSiO _{3(s)} + 1/4 CO _{2(g)} → 1/4 MgCO _{3(s)} + 1/4 SiO _{2(s)}	-21.22	-8.27	(8)
Dehydration of chrysothile Mg₃Si₂O₅(OH)_{4(s)}			
Mg ₃ Si ₂ O ₅ (OH) _{4(s)} + 2SiO _{2(s)} → Mg ₃ Si ₄ O ₁₀ (OH) _{2(s)} + H ₂ O _(l)	-4.40	-12.30	(9)

Individual values for reactants and products are taken from Robie and Hemingway's 1995 tables, at 298.15 K and 1 bar (Robie and Hemingway 1995)

Values for SiO₂ are those of quartz and for Mg₃Si₂O₅(OH)₄ those of the serpentine chrysothile. Entropy values for (1) and (5) are calculated considering S⁰(H₂) = 130.45 J.K⁻¹.mol⁻¹

Table 2 Redox equations constructed for this article upon diagrams drawn in the associated references. In each case, the total concentration of dissolved iron is 10^{-6} mol.kg⁻¹. H₂S is dissolved in water. pH values are approximate, depending on concentrations

Redox equations	T °C	pH	Eq.	References
Fe ^{II} (OH) ₃ ⁻ + H ₂ O → Fe ^{III} (OH) ₄ ⁻ + 1/2 H ₂	350	11.5 to 14	(10)	Cook and Olive 2012
Fe ²⁺ + 4/3H ₂ O → 1/3Fe ₃ O ₄ + 1/3H ₂ + 2H ⁺	25	8.5	(10)'	Pourbaix 1963
FeS + 4/3H ₂ O → 1/3Fe ₃ O ₄ + H ₂ S + 1/3H ₂	250	3.5 to 8	(11)	Macdonald 1992
FeS + H ₂ S → FeS ₂ + H ₂	25	5.4 to 9.5	(12)	Macdonald 1992
Fe ²⁺ + 1/4O ₂ + H ⁺ → Fe ³⁺ + 1/2H ₂ O	25	< 8.5	(13)	Pourbaix 1963
Fe ²⁺ + 1/4O ₂ + H ⁺ → Fe ³⁺ + 1/2H ₂ O	350	< 4.2	(14)	Cook 2012
H ₂ S + 2O ₂ → H ₂ SO ₄	250	0 to 8.5	(15)	Macdonald 1992
	25	< 3.6		
FeS + 1/6O ₂ + H ₂ O → 1/3Fe ₃ O ₄ + H ₂ S	250	3.7 to 8	(16)	Macdonald 1992
(H ₂ S can transform into H ₂ SO ₄)				
Fe ₃ O ₄ + 1/4O ₂ → 3/2Fe ₂ O ₃	250	2.5 to 12	(17)	Macdonald 1992
FeS + 1/4O ₂ + H ₂ O → 1/2Fe ₂ O ₃ + H ₂ S	250	3.7 to 8	(18)	Macdonald 1992
(H ₂ S can transform into H ₂ SO ₄)				
FeS + 11/5O ₂ + H ₂ O → 1/5Fe ₃ O ₄ + 1/5Fe ₂ O ₃ + H ₂ SO ₄	250	3.7 to 8	(19)	Macdonald 1992
2Fe ²⁺ + 1/2O ₂ + 3H ₂ O → 2Fe(OH) ₂ ⁺ + 2H ⁺	250	< 3	(20)	Macdonald 1992
	25	< 4		
FeS + H ₂ S + 1/2O ₂ → FeS ₂ + H ₂ O	25	5 to 12	(21)	Macdonald 1992
(3S(-I)–S(-I)) ⁴⁻ + O ₂ → 3S(-II) ²⁻ + S(+VI)O ₂ ²⁺			(22)	
2FeS ₂ + 3/2O ₂ + 5H ₂ O + 2H ⁺ → 2Fe(OH) ₂ ⁺ + H ₂ SO ₄ + 3 H ₂ S	25	5	(23)	

This $\text{Fe}(\text{OH})_4^- / \text{Fe}(\text{OH})_3^-$ redox equation which can be written from a E-pH diagram drawn at 350 °C, 25 MPa, cannot be written from the diagram that Pourbaix drew at 25 °C, for the same concentration (Fig.4 p. 312 of Pourbaix 1963). Instead, at 25 °C, it is magnetite which forms with release of H_2 at pH limited around 8.5, following eq. (10)' of Table 2.

We deduce that, in anoxic conditions, at high temperature and high pH, ferrous ion transforms into ferric ion under the form of goethite, with release of H_2 , and that at 25 °C and pH \sim 8.5, it is magnetite which forms in association with H_2 . This observation can most probably be related to low temperature serpentinization which has been reported to occur in some geological sites. The E-pH diagram drawn by Pourbaix at 25 °C is also interesting because lines are traced for different concentrations, showing that pH values depend on concentrations. For a concentration of dissolved iron $10^{-2} \text{ mol.kg}^{-1}$, magnetite is produced at pH \sim 6.5. Thus information on redox equations and stability domains can be extracted from E-pH diagrams, but with cautiousness.

The dissolution of CO_2 in water does not change the appearance of the E-pH diagrams. By comparison with diagrams constructed for the ternary system iron, water and carbon dioxide, between 25 °C and 150 °C, at concentrations of dissolved iron $10^{-5} \text{ mol.kg}^{-1}$, and carbonates 10^{-2} , 10^{-3} , $10^{-4} \text{ mol.kg}^{-1}$ (Chivot 2004), it can be deduced that the presence of CO_2 does not change the appearance of the Fe- H_2O diagrams and that eq. (10) of Table 2 may most probably be written for the ternary system Fe- CO_2 - H_2O at 350 °C and 25 MPa. The presence of CO_2 does not alter the conclusion that dissolved goethite $\text{Fe}(\text{OH})_4^-$ is formed at high pH, with release of H_2 .

Consequently in anoxic ferromagnesian silicate terrains, upon the Cook and Olive diagram, the ferric oxide hydroxides $\text{FeO}(\text{OH})$, including goethite and lepidocrocite, are produced under their dissolved form $\text{Fe}(\text{OH})_4^-$, together with H_2 , following eq. (10), at high pH above \sim 11.5 and for temperature and pressure near the critical point of water which bears the values 374 °C, 22.1 MPa for pure water.

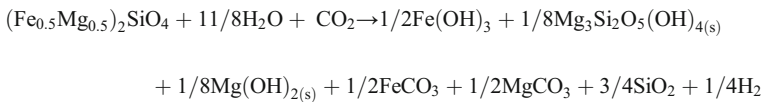
The thermodynamic equations of Table (1) which are related to the redox eq. (10), for the geological oxidative hydrolyses of fayalite and ferrosilite, in the absence of O_2 , are (1)' and (5)'. Reactions are endothermic and require a hydrothermal system to occur. They can be constructed from E-pH diagrams at 350 °C and not at 25 °C. A calorimetric experiment conducted up to 685 °C, showed that natural goethite, with ca 13% H_2O attached to $\text{FeO}(\text{OH})$ and no titanomagnetite neither pyrrhotite but perhaps trace amounts of organic matter, converts into hematite between 260 °C and 360 °C with trace amounts of magnetite above 400 °C. "At 685°C, the magnetic mineralogy was usually dominated by magnetite" (Dekkers 1990). Another experiment conducted on heating amorphous ferric hydroxide in sealed ampoules, between 100 and 200 °C, produced hematite only at pH 0.8 to 2.6, hematite and goethite at pH 8.0 to 10.0, and goethite only at pH 10.5 to 10.8 (Christensen 1968).

Thus the hydrolyses of fayalite and ferrosilite in the absence of oxygen lead preferentially to ferric trihydroxide and ferric oxide hydroxides, following eq. (1)' and (5)' and after dehydration to hematite, instead of magnetite, following eqs. (1)'' and (5)'' which are precisely more endothermic than eqs. (1) and (5).

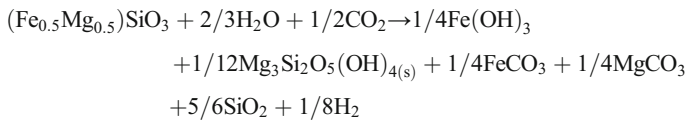
Consequently, the ferric ions formed during the anoxic hydrothermal hydrolysis of the iron endmembers of olivine and pyroxene seem incorporated into iron oxides/hydroxides but not magnetite. They can also be incorporated into the structures of the hydrolysis products of the magnesium endmembers to form Fe(III)-phyllosilicates. For instance, the T-O phyllosilicate chrysotile $\text{Mg}_3\text{Si}_2\text{O}_5(\text{OH})_4$, which may be represented as $[(3\text{Mg})^{6+} (\text{Si}_2\text{O}_5)^{2-} (4\text{OH})^4]$, may form as $(\text{Mg}^{\text{II}}, \text{Fe}^{\text{III}})_3\text{Si}_2\text{O}_5(\text{OH})_4$ or $(\text{Al}^{\text{III}}, \text{Fe}^{\text{III}})_2\text{Si}_2\text{O}_5(\text{OH})_4$ and the T-O-T phyllosilicate talc $\text{Mg}_3\text{Si}_4\text{O}_{10}(\text{OH})_2$, represented as $[(3\text{Mg})^{6+} (\text{Si}_4\text{O}_{10})^{4-} (2\text{OH})^2]$, may form as

$(\text{Mg}^{\text{II}}, \text{Fe}^{\text{II}})_3\text{Si}_4\text{O}_{10}(\text{OH})_2$ or $(\text{Al}^{\text{III}}, \text{Fe}^{\text{III}})_2\text{Si}_4\text{O}_{10}(\text{OH})_2$. The hydrogen which is released during the serpentinization reactions accompanies the formation of ferric oxides/hydroxides at 350 °C and magnetite at 25 °C.

Calculations of thermodynamic functions for the exothermic reactions of the serpentinization process lead to high values. The enthalpy of forsterite hydrolysis (eq.2) is: $\Delta_r H^0 = -288.2$ kJ/kg of forsterite Mg_2SiO_4 and the enthalpy of forsterite carbonation (eq.4) is: $\Delta_r H^0 = -1260$ kJ/kg of forsterite Mg_2SiO_4 . The enthalpy of fayalite carbonation (eq.3) is: $\Delta_r H^0 = -772$ kJ/kg of fayalite Fe_2SiO_4 . The enthalpy of serpentinization for $(\text{Fe}_{0.5}\text{Mg}_{0.5})_2\text{SiO}_4$ olivine, is calculated by summation of enthalpies of the 4 eqs. 1', 2, 3 and 4: $\Delta_r H^0 = -90.3$ kJ/mol of $(\text{Fe}_{0.5}\text{Mg}_{0.5})_2\text{SiO}_4$ olivine, which corresponds to $\Delta_r H^0 = -524.35$ kJ/kg of $(\text{Fe}_{0.5}\text{Mg}_{0.5})_2\text{SiO}_4$ olivine and to the following global equation:



The enthalpy of enstatite hydrolysis (eq.6) is: $\Delta_r H^0 = -206.8$ kJ/kg of enstatite MgSiO_3 and the enthalpy of enstatite carbonation (eq.8) is: $\Delta_r H^0 = -845.4$ kJ/kg of enstatite MgSiO_3 . The enthalpy of ferrosilite carbonation (eq.7) is: $\Delta_r H^0 = -590.5$ kJ/kg of ferrosilite FeSiO_3 . The enthalpy of serpentinization for $(\text{Fe}_{0.5}\text{Mg}_{0.5})\text{SiO}_3$ pyroxene, is calculated by summation of all enthalpies of eqs. 5', 6, 7 and 8: $\Delta_r H^0 = -43.98$ kJ/mol of pyroxene $(\text{Fe}_{0.5}\text{Mg}_{0.5})\text{SiO}_3$, which corresponds to $\Delta_r H^0 = -378.61$ kJ/kg of pyroxene $(\text{Fe}_{0.5}\text{Mg}_{0.5})\text{SiO}_3$, and to the following global equation:



When peridotite is composed mainly of ferrosilite, the enthalpy of the serpentinization process becomes at the extreme the summation of the enthalpies of eqs. (5)' and (7), and takes the value of -266.05 kJ/kg of ferrosilite which should correspond to a lower temperature.

Thus, the calculated enthalpies and free enthalpies of the elementary reactions of hydrolysis and carbonation of the ferromagnesian silicates show that oxidation of ferrous iron in anoxic water is an endothermic process. E-pH diagrams show that at 350 °C this oxidation occurs at high pH ~ 11.5 to 14, with production of the ferric tetrahydroxide anion and at 25 °C around pH 8.5 with production of magnetite.

From these analyses, it can be inferred that, on geological terrains, the anoxic serpentinization process gives primary products which are ferric phyllosilicates, ferric trihydroxide, dissolved goethite, and after dehydration the ferric oxide hydroxides goethite $\alpha\text{-Fe}(\text{III})\text{O}(\text{OH})$ and lepidocrocite $\gamma\text{-Fe}(\text{III})\text{O}(\text{OH})$, and hematite. Magnetite is produced in trace amounts as a secondary product.

Magnetite at 250 °C and Pyrite at 25 °C with No Carbonates as Products of the Anoxic Hydrolysis of Ferrous Monosulfides Rocks

A thermodynamic equilibrium E-pH diagram has been drawn, at 250 °C, for the ternary system Fe-S-H₂O in high salinity geochemical brines with "activities of dissolved metal containing species arbitrarily set to $10^{-4}(m)$ " (Fig.2 of Macdonald 1992). This diagram

displays many species and is consequently confusing. However it shows clearly a stability domain for magnetite and it seems plausible to write the redox eq. (11) of Table 2 considering the oxidation of the ferrous sulfides, mackinawite/troilite/pyrrhotite Fe(II)S(-II) into magnetite Fe(II)Fe(III)₂O₄. At 250 °C, magnetite and H₂ are produced at pH ~3.5 to 8, in the absence of oxygen, not because of transformation of ferrosilicates but because of transformation of ferrosulfides and a change in the oxidation number of iron(II) to iron(III). Enthalpy functions calculated at 298.15 K and 1 bar for this eq. (11) considering the reactant troilite, show that the reaction is endothermic ($\Delta_r H^0 = +89.57$ kJ/mol of FeS) and does not proceed spontaneously ($\Delta_r G^0 = +46.47$ kJ/mol of FeS). An hydrothermal system is required to produce magnetite from mackinawite/troilite/pyrrhotite, for instance the hydrolyses and carbonations of olivine and pyroxene as calculated above, or heat from magma or hydrothermal sources, or the fall on Earth or elsewhere of asteroidal type objects.

The diagram Fe-S-H₂O drawn at low temperature 25 °C (Fig.1 of Macdonald 1992) is quite different as far as the magnetite stability domain is concerned. Production of Fe₃O₄ associated with H₂ production occurs around pH 12, and it is pyrite Fe(II)S(-I)₂ which forms between pH ~5.4 to 9.5 with emission of H₂, in the absence of oxygen, in an exothermic and spontaneous reaction ($\Delta_r H^0 = -48.3$ kJ/mol of FeS, $\Delta_r G^0 = -23.8$ kJ/mol of FeS) (eq.12).

Our theoretical observation upon E-pH diagrams, that ferrous sulfides produce pyrite at low temperature is confirmed by laboratory experiments conducted between 25 °C and 125 °C on anoxic oxidation of iron(II) monosulfide (Rickard 1997). And our theoretical observation that ferrous sulfides produce magnetite at 250 °C, in the absence of oxygen, is confirmed by experiments conducted on mackinawite, i.e. tetragonal iron(II) monosulfide, which is heated up to 410 °C and studied by in situ X-ray diffraction and transmission electron microscopy, TEM (Lennie et al. 1997). In this last experiment, greigite, the ferrous ferric polysulfide Fe₃S₄ forms at 70 °C for one sample and at 100 °C for another one. The diffraction patterns show that greigite decomposes into the ferrous monosulfide pyrrhotite and into magnetite above 245 °C. Eq. (11) can explain the formation of magnetite in the above experiments, starting with iron(II) monosulfide and with greigite as intermediate product.

Recently, in 2016, has been published a study by computational methods of the anoxic oxidation of greigite with production of dissolved H₂S and magnetite. It is shown that the partial oxidation of Fe₂₄S₃₂ by water with replacement of S (forming H₂S) by O (from H₂O) is thermodynamically favorable and produce Fe₂₄S₃₁O (Santos-Carballal et al. 2016).

Other laboratory heating experiments have been conducted up to 250 °C, on claystones put into small flasks in confined atmosphere, where it is demonstrated that laboratory heating of clays trigger the formation of magnetic minerals. Pyrrhotite seems to dominate at low temperature and magnetite overshadows the magnetic input of pyrrhotite at T above 85 °C up to 250 °C (Kars et al. 2012; Aubourg and Pozzi 2010). These experiments prove the predominance of pyrrhotite below 85 °C and magnetite above 85 °C up to 250 °C. Eq. (11) can also explain the formation of magnetite in these experiments on heated clays and also the remagnetization of claystone-type rocks during <4 km burial. It is however to be noticed that goethite was observed in the clay sample before heating. Considering our elementary reactions which produce ferric tetrahydroxide and goethite or lepidocrocite (eq. 1', 5') during serpentinization, the goethite in the clay sample can be a product of the altered minerals which formed the clay sample. Goethite during heating dehydrates mainly into non-magnetic hematite and also into small amounts of magnetite, as described in §1.1. for the calorimetric

experiment (Dekkers 1990), but not below 400 °C. Thus, the magnetic products formed in the clay heating experiments seem to arise mainly from the anoxic oxidation of pyrrhotite following eq. (11).

From the exothermic enthalpies calculated in §1.1. for the ferromagnesian silicate hydrolyses and carbonations compared to the endothermic values obtained for the iron(II) monosulfide hydrolysis, it may be inferred that hydrolysis/oxidation of ferrous sulfide can proceed in symbiosis with hydrolyses and carbonations of ferromagnesian silicates during the process of serpentinization. Since FeS produces Fe₃O₄ only at very high pH ~12 at 25 °C and at pH ~3.5 to 8 at 250 °C, it is plausible to propose by extrapolation that pH of magnetite formation from ferrous sulfide decreases when temperature increases. That might explain the pH value ~3 at the Rainbow field which vents fluids at ~365 °C and shows sulfide chimneys, and also at other low pH hydrothermal vents of the spreading ridges, as discussed in §3.2.

The observation of magnetite as unique ferric compound in the absence of carbonates, in an iron(II) monosulfide hydrothermal geological site may lead to the conclusion that anoxic water hydrolyzed the iron-sulfide rocks at that location. This process of anoxic hydrolysis/oxidation of troilite following eq. 11 of Table 2 can explain magnetic anomalies associated with sulfur smells as perhaps for the Chelyabinsk asteroid (Popova et al. 2013 p101) and magnetic anomalies associated with production of dissolved H₂S as discussed for hydrothermal venting fields in §4.3.

The 2007 Seyfried experiment on serpentinization of lherzolite type peridotite produced "only a trace level of H₂S, 0.06 mmol/kg", after 700 h, at pH not determined but which can be inferred most probably below 8. This pH value corresponds to our proposition of eq. (11) for the formation of magnetite together with hydrogen sulfide. Since no sulfides are reported to be present inside the starting lherzolite, and since only traces of hydrogen sulfide and "only trace quantities of magnetite (~0.014%)" are detected, it can be suggested that in this experiment, the traces of hydrogen sulfide and magnetite arise from the hydrolysis of traces of iron monosulfides which were present in the lherzolite. Thus it seems plausible to propose that, in a general way, magnetite arises from iron(II) monosulfide hydrolysis following our eq. (11) instead from olivine and/or pyroxene hydrolyses. This remark leads to the conclusion that hydrolyses of ferromagnesian silicates follow rather our eqs. (1)' and (5)' with formation of ferric ions inside ferric trihydroxide as product, which can be written as hydrated goethite, FeO(OH)H₂O, which can consecutively dehydrate into goethite, lepidocrocite and hematite. The ferric ions can also integrate the structures of the formed phyllosilicates as already discussed in §1.1. Indeed Mössbauer spectroscopy applied to the serpentine produced in the cited lherzolite seawater experiment shows "two doublets indicating the presence of both Fe³⁺ and Fe²⁺ in the octahedral layer of the serpentine".

The serpentinization experiment on uncrushed harzburgite cited in the introduction (Klein et al. 2015) reports that "neither brucite nor talc precipitated during the experiment" and that the experiment did not go to completion. As it is shown by eq. (9) formation of talc from serpentine requires a solution super saturated in SiO₂. It can thus be suggested that lizardite and chrysotile kept all silicon and oxygen. The report that no brucite was detected leads to the suggestion that all OH-Mg-OH bonds are most probably integrated inside the structures of the observed lizardite and chrysotile. Crystal structures of brucite, chrysotile and talc have been generated using the Vesta software and standard mineral structures from the American mineralogist crystal structure data base (Li et al. 2014). Fig. 1. of this cited article shows that "brucite, with its octahedral structure, has a lattice configuration that is similar to the Mg-bearing octahedral layers in phyllosilicates." It can be easily observed in this figure that the T-O phyllosilicate chrysotile Mg₃Si₂O₅(OH)₄ is composed of a tetrahedral layer of Si and O, and

an octahedral layer of Mg and O similar to brucite, while the T-O-T phyllosilicate talc $\text{Mg}_3\text{Si}_4\text{O}_{10}(\text{OH})_2$ is composed of an octahedral layer of Mg and O, integrated inside two tetrahedral layers of Si and O. The structures of lizardite and chrysotile are compositionally similar but can be precisely distinguished by analyzing the vibrations of the OH-Mg-OH groups with FT-Raman spectroscopy. *"The bands produced by vibrations of the SiO_4 tetrahedra or by silicon-oxygen linkages appear at frequencies very close to those detected in the chrysotile spectra...The vibrations of OH-Mg-OH groups appear to be shifted to higher frequencies on the lizardite spectrum 630 cm^{-1} , when compared to the vibrations of the same groups in chrysotile, 620 cm^{-1} "* (Rinaudo et al. 2003). Thus, since serpentinization was not complete in the harzburgite experiment, it is plausible to suggest that both lizardite and chrysotile captured the $\text{Mg}(\text{OH})_2$.

This serpentinization experiment starts with the peridotite rock harzburgite which contains the sulfides "*pentlandite $\text{Ni}_{4.9}\text{Fe}_{4.1}\text{S}_8$* " and "*pyrrhotite with approximately of stoichiometric composition*" (i.e. troilite), which are "*irregularly distributed within the rock*". It is observed that "*when fluid accessed the sulfides, heazlewoodite and magnetite precipitated...pentlandite is found together with magnetite*". Heazlewoodite formula is Ni_3S_2 . Ni is known to be not easily incorporated into magnetite and it has been shown that pyrrhotite, which is formed during troilite oxidation, is enriched in Ni (Bullock et al. 2005). Thus it is possible to suggest that, in the harzburgite seawater experiment, magnetite forms from the hydrolysis/oxidation of pentlandite and pyrrhotite/troilite, instead from the hydrolysis of olivine. The experiment is conducted at $350\text{ }^\circ\text{C}$ and 35 MPa, and our conclusion about sulfide hydrolysis forming magnetite, arises from E-pH diagrams drawn at $250\text{ }^\circ\text{C}$ for Fe-S- H_2O systems and at $350\text{ }^\circ\text{C}$ and 25 MPa for the Fe- H_2O system.

Another experiment conducted on surfaces of ground pyrrhotite oxidized by water which is distilled, deionized and deoxygenated by sonication, at pH 5.5 and at ambient temperature, formed 35% FeOOH , 5.5% S-rich sulfides (S-S bonds) and no sulfates (Jones et al. 1992). The formed goethite is difficult to explain without the action of oxygen which would also lead to sulfates. However, the temperature and pH correspond to eq. (12) with production of the S-rich sulfide pyrite. If some oxygen is remaining in the water, it could be incorporated into FeO as discussed in §2.3. for pyrite oxidation, and the small amount of oxygen would not be sufficient to oxidize H_2S into sulfates.

Consequently, upon our theoretical analyses and the confirming experiments, it appears plausible to propose that during the high temperature ($350\text{ }^\circ\text{C}$ – $250\text{ }^\circ\text{C}$) serpentinization reactions of peridotite rocks, magnetite is mainly produced by the hydrolyses of the ferrous monosulfides following eq. (11) that we have constructed and not by the hydrolyses of the ferromagnesian silicates olivine and pyroxenes.

Oxic Alteration of Ferromagnesian Silicates and Ferrous Monosulfide Rocks

Radiolyzed Water and Molecular Oxygen

Molecular hydrogen is produced during irradiation of water by ionizing radiation, and production is exponential in supercritical water. Water radiolysis is a source of the reducing species, H_2 , the hydrogen atom H^\bullet , the hydrated electron e^-_{aq} , and also the following oxidizing species, hydrogen peroxide H_2O_2 , the hydroxyl radical OH^\bullet , the hydroperoxyl radical HO_2^\bullet and O_2 (Buxton 2008; Baldacchino and Hickel 2008). In boiling water reactors (BWR) and pressurized water reactors (PWR), which are operated at constant temperature (280 – $325\text{ }^\circ\text{C}$)

and constant pressure (15–20 MPa), the water is exposed to a strong radiation field composed of gamma rays and neutrons and two radiolysis products of water are O_2 and H_2O_2 . It is the same for the supercritical water reactors (SCWR). Injection of H_2 into the coolant converts O_2 and H_2O_2 into H_2O by radiolytic processes (Lin et al. 2010). A modeling of radiolysis control for a Canadian SCWR has been recently proposed by H_2 addition (Huang et al. 2016). Thus O_2 is a product of water radiolysis.

The species H_2 , H^\bullet , e^-_{aq} , H_2O_2 and OH^\bullet are produced when the energy absorbed by water is low, i.e. when radiations are in the range of low-linear energy transfer (low-LET) radiations. Low-LET radiation is produced by gamma radiation, accelerated electrons and high-energy X-rays, and high-LET radiation is produced by neutrons and heavy ions including alpha particles (Le Caër 2011). As for example, LET values are $0.2\text{--}0.3\text{ keV}\cdot\mu\text{m}^{-1}$ for ^{60}Co γ -rays and $140\text{ keV}\cdot\mu\text{m}^{-1}$ for 5.3 MeV alpha particles (^{210}Po) (Ferradini and Jay-Gerin 1999) and $0.3\text{ keV}\cdot\mu\text{m}^{-1}$ for a beam of 300 MeV protons in liquid water at 25° (Sanguanmith et al. 2012) and $34.8\text{ keV}\cdot\mu\text{m}^{-1}$ for a beam of 2 MeV protons (Crumière et al. 2013). As LET increases, the radical density increases, the probability of encounter between O^\bullet and OH^\bullet increases and leads to an enhanced production of HO_2^\bullet which in turn reacts with OH^\bullet to form O_2 and H_2O . Production of O_2 is proposed to dominate for LET larger than $300\text{ keV}\cdot\mu\text{m}^{-1}$ (Gervais et al. 2005) and it is experimentally proven that an alpha beam with an incident energy of 3.7 MeV produces O_2 within a radiolysis zone of $25\text{ }\mu\text{m}$ (Liedhegner et al. 2011). Molecular oxygen can thus be a product of water radiolyzed by high-LET. O_2 was earlier proposed as a water radiolysis product in low-LET radiolyses with ^{60}Co γ -rays (Daniels and Wigg 1966). However it was noticed that confusion might exist between O atoms and O_2 molecules.

In Kobayashi experiments with 10 cm beams, LET values were $2.2\text{ keV}\cdot\mu\text{m}^{-1}$ for He, $13\text{ keV}\cdot\mu\text{m}^{-1}$ for C and $30\text{ keV}\cdot\mu\text{m}^{-1}$ for Ne. These excitations sources are below $300\text{ keV}\cdot\mu\text{m}^{-1}$ and the beams are directed in the gas phase above liquid water. Molecular oxygen is not produced. High-LET radiation sources are found in cosmic radiation together with low-LET and also in radioactive rocks with alpha-emitters. It is most probable that at the surface of comets or planets, when and where water is locally set in the liquid state, there is formation of O_2 in the radiolyzed water. In the interior of rocky objects such as planets, comets, asteroids, meteorites, the radionuclides ^{238}U , ^{235}U , ^{232}Th , which are alpha emitters, allow in their vicinity, formation of O_2 in water. In addition, the following alpha emitters can also be considered: ^{142}Ce ^{144}Nd ^{147}Sm ^{148}Sm ^{152}Gd ^{174}Hf ^{186}Os ^{190}Pt . In locations where T and P reach the values of high subcritical water, as in hydrothermal vents, or in some high-T serpentinization reactions, or impact heat, O_2 is produced when high-LET alpha emitter's radionuclides are present.

Magnetite, Ferric Trihydroxide, Ferric Oxide Hydroxides and Hematite with No Carbonates and No Sulfates as Products of the Oxidic Hydrolysis of Ferromagnesian Silicate Rocks at 25 °C and 350 °C

Upon the E-pH diagram drawn at low temperature, 25°C , for total concentration of dissolved iron $10^{-6}\text{ mol}\cdot\text{kg}^{-1}$ (Pourbaix 1963), eq. (13) can be deduced for oxidation of Fe(II) by oxygen. The iron end member of the ferromagnesian silicate can be oxidized into ferric iron, under the form of dissolved goethite $\text{FeO}(\text{OH})\text{H}^+$, $\text{Fe}(\text{OH})_2^+$, below pH ~ 1.8 , hematite at pH ~ 1.8 to 7.2 and magnetite at pH ~ 7.2 to 8.5. The cation $\text{Fe}(\text{OH})_2^+$ is the dissolved species of $\text{Fe}(\text{OH})_{3(s)}$ in acidic water and the anion $\text{Fe}(\text{OH})_4^-$ is the dissolved species in alkaline water, as described in §1.1.

The E-pH diagram drawn at 350 °C and 25 MPa for 10^{-6} mol.kg⁻¹ total concentration of dissolved iron (Cook and Olive 2012), shows, below pH ~9.2, the same kind of shape than at 25 °C. Below pH ~4.2, the potential line of the O₂/O⁻ couple is higher than the potential line of the Fe³⁺/Fe²⁺ couple; in the presence of O₂, Fe(II) transforms into Fe(III) following eq. (14) of Table 2 which is the same than eq. (13) at 25 °C, but at lower pH. There is production of the dissolved goethite in its acidic form, Fe(OH)₂⁺, below pH ~1.9, hematite between pH ~1.9 and ~2.5 and magnetite between pH ~2.5 and ~4.2.

Calorimetric experiments as described in §1.1. for anoxic reactions show that after dehydration, dissolved goethite can lead to hematite and traces of magnetite above 400 °C. The following two experiments show also dehydration of goethite into hematite in oxic conditions. Pure synthetic powdered goethite, α-FeO(OH) was progressively transformed into hematite, in a flow of air heated up to 800 °C, with production of Fe_{2-x/3}(OH)_xO_{3-x}, an intermediate phase. "The thermal analysis showed that our sample had an excess of water (likely surface adsorbed water) that is lost at approximately 70°C... the decomposition of goethite started at 200°C and concluded at about 270°C... the structure of phase formed from the decomposition of goethite was non-stoichiometric hematite... at 800°C, protohematite was almost completely converted into hematite" (Gualtieri and Venturelli 1999). The dehydration of synthetic goethite heated in air, has been also studied, by induced magnetization and X-ray diffraction, between 155 °C and 610 °C. An intermediate spinel phase assigned to magnetite was observed between 255 and 405 °C and only hematite was found at 500 and 610 °C (Özdemir and Dunlop 2000).

Thus upon E-pH diagrams, ferromagnesian silicate terrains which contain radioactive rocks and/or are submitted to cosmic radiation, lead to the formation of goethite/lepidocrocite, hematite and magnetite. The endothermic reactions of hydrolysis of ferrous silicate (eq. 1, 1', 1'', 5, 5', 5'') have not to be considered for this oxidation, since water is oxygenated. Thus, the exothermic reactions of carbonation are not necessary to produce the ferric compounds from the anoxic endothermic hydrolyses, and carbonates are not formed. Consequently the observation of goethite/lepidocrocite, hematite, magnetite without carbonates, in ferromagnesian silicate terrains containing radioactive rocks and/or submitted to cosmic radiation, leads to the hypothesis that oxygenated water existed at that location either at 25 °C or higher, 350 °C. Molecular hydrogen which formed during water radiolysis might have escaped in conditions which are not necessarily hydrothermal.

Magnetite at 250 °C and Pyrite at 25 °C, Associated to Hematite, Ferric Trihydroxide, Ferric Oxide Hydroxides, Sulfates and No Carbonates, as Products of the Oxic Hydrolysis of Ferrous Monosulfide Rocks

From the ternary diagram drawn for the system Fe-S-H₂O at 250 °C (Macdonald 1992) equations representing the interaction with oxygen can also be extracted: eq. (15) which shows transformation of hydrogen sulfides H₂S and HS⁻ into sulfate at pH 0 to ~8.5; eq. (16) which shows transformation of ferrous sulfides FeS, such as mackinawite, troilite and pyrrhotite, into magnetite at pH ~3.7 to 8 without considering oxidation of H₂S into sulfate; eq. (17) which shows transformation of magnetite into hematite at pH ~2.5 to 12; eq. (18) which shows transformation of FeS into hematite at pH ~3.7 to 8 without considering oxidation of H₂S into sulfate. Eq. (19) summarizes the oxidation of FeS into magnetite, hematite and sulfate in oxygenated water. The dissolved form of goethite, Fe(OH)₂⁺, not indicated in the diagram, may also form in acidic pH, below ~3, following eq. (20). Eq. (16) represents the oxidation of iron(II) monosulfide by oxygen at 250 °C. Enthalpy functions calculated at

298.15 K and 1 bar and troilite, for this eq. (16) show that the reaction is exothermic ($\Delta_r H^0 = -5.70$ kJ/mol of FeS) and proceeds spontaneously ($\Delta_r G^0 = -32.57$ kJ/mol of FeS). An hydrothermal system is not required to produce magnetite from mackinawite/troilite/pyrrhotite at 250 °C, in the presence of oxygen as it is required for the anoxic hydrolysis.

The Macdonald 1992 diagram drawn at 25 °C, shows that in the presence of oxygen, the sulfur S(-II) of iron(II) monosulfide is oxidized into the sulfur S(-I) of pyrite in a S-S bond, at pH ~5 to 12 following eq.(21) and to magnetite only at very high pH > ~12. The diagram shows clearly that magnetite is located far away in the high pH range above ~12 and that pyrite in the presence of oxygen can be oxidized into hematite and ferric trihydroxide at pH below ~12 and into the acidic dissolved goethite $\text{Fe}(\text{OH})_2^+$ below pH ~4. Sulfate can form below pH ~3.6. Formation of dissolved goethite follows eq. (20) as at 250 °C.

The pyrite oxidation mechanism is complex since both the sulfur atoms of the dimer $\text{S}(-\text{I})_2^{2-}$ and the iron (II) are concerned and the redox equation difficult to write. A recent article studies the process of adsorption of O_2 and H_2O on pyrite surfaces (Dos Santos et al. 2016) and is related to the experiment conducted at ambient temperature and pH 5, which indicates "water as the primary source of oxygen in the sulfate product, while the oxygen atoms in the iron oxyhydroxide product are obtained from dissolved molecular oxygen" (Usher et al. 2004). Following these experimental results and the E-pH diagrams, I suggest the redox eqs. (22) and (23) for pyrite oxidation by O_2 at low temperature, 25 °C and pH 5. Since the medium is acidic the observed dissolved ferric oxide hydroxide should be under the species $\text{Fe}(\text{OH})_2^+$. As written in eq. (23), one oxygen of $\text{Fe}(\text{OH})_2^+$ comes from dissolved molecular oxygen and one comes from water. Two oxygen of the sulfate come from O_2 (eq. 22) and two from water. Two dimers S_2^{2-} , with oxidation number - 1 for each sulfur atom, transform into one S(+VI) of the sulfate and three S(-II) of the hydrogen sulfide. The global eq. (23) can be written. It shows production from pyrite of sulfate and of the species goethite dissolved in acidic water. The three H_2S can further oxidize into sulfate upon eq. (15).

Thus, at 25 °C, iron(II) monosulfide is oxidized by oxygen mainly into pyrite and also sulfates and hematite and goethite/lepidocrocite. At 250 °C, iron(II) monosulfide is oxidized by oxygen mainly into magnetite and also sulfate, hematite and goethite/lepidocrocite.

On geological terrains, mackinawite/troilite/pyrrhotite oxidation by oxygen at low temperature, ~25 °C, would lead mainly to pyrite and also to sulfates, and to deposits of goethite and/or lepidocrocite $\text{FeO}(\text{OH})$ and hematite Fe_2O_3 , which is dehydrated $\text{FeO}(\text{OH})\text{H}_2\text{O}$ also represented as $\text{Fe}(\text{OH})_3$. Magnetite instead of pyrite, would be deposited in hydrothermal environments together with sulfates, hematite and goethite/lepidocrocite.

A related experiment shows that troilite oxidation in oxygen-bearing acidic solutions at $T \sim 35$ °C, led at pH ~ 5 to poorly ordered solid phases assigned to sulfur-rich compounds such as polysulfide, and to amorphous ferric trihydroxide, goethite, lepidocrocite and minor sulfate (Chirita et al. 2008). The sample contained mostly pyrrhotite (Fe_7S_8) and troilite (FeS), together with minor amounts of pyrite (FeS_2). It is suggested that as the reaction advances "the formed polysulfide can undergo a rearrangement" and that an increase in "the amount of dissolved iron and pH leads to precipitation of amorphous $\text{Fe}(\text{OH})_3$, lepidocrocite and goethite". This experiment is related to eq. (21) which represents the oxidation of troilite with production of pyrite, which in turn oxidizes following eq. (22) and (23) to produce sulfate and the acidic form of dissolved goethite $\text{Fe}(\text{OH})_2^+$ which leads further on to goethite/lepidocrocite and hydrated goethite $\text{FeO}(\text{OH})\text{H}_2\text{O}$ which is ferric trihydroxide. Thus the cited experiment confirms our theoretical results.

Another experiment on FeS oxidation at high temperature was conducted with magnetic dipole moments measurements during heating of pyrrhotite rocks from Massif Central/France.

It is demonstrated that magnetite forms at 400 °C: "*Thermal evolution of susceptibility has been followed in air or in vacuum with no substantial difference found*" (Bina et al. 1991). This experiment confirms our theoretical observation that magnetite forms in anoxic (eq. 11) and oxic (eq. 19) oxidation of FeS at 250 °C.

Also magnetic dipole moments studies of iron meteorites containing troilite and pyrrhotite heated in sealed tubes showed Curie temperature at 580 °C and X-ray analysis led to magnetite. Since atmospheric pressure was low ($P < 0.1$ mmHg) this observation was reported as difficult to understand (Lovering and Parry 1962). However, in our anoxic and oxic discussions, we showed that magnetite form in both cases at 250 °C and not at 25 °C. It is the temperature which is the dominant parameter for iron(II) monosulfide transformation into magnetite. In the case of this experiment, which can be considered in anoxic conditions, eq.(11) can most probably be evoked.

Finally, oxidation of magnetite in air which was heated at 750 °C to 900 °C, resulted in hematite formation (Monazam et al. 2014).

Geobiotropic Signatures

The minerals that we have found in association with release of H₂, as products of anoxic and oxic alteration of ferromagnesian silicate and iron(II)-monosulfide rocks, are summarized in Table 3. Our analyses seem widely confirmed by results of ancient and recent experiments. Thus it is plausible to write that minerals of Table 3 are geological signatures of anoxic and oxic hydrolyses. We show that magnetite is not a direct product of the high-T (350 °C) serpentinization process, but rather a product of the low-T (25 °C) serpentinization at a specific pH around 8.5 (§ 1.1.), and that the product of the anoxic hydrolysis at 250 °C and low pH ~3.5–8 of iron(II) monosulfide, mackinawite/troilite/pyrrhotite is magnetite and at 25 °C pyrite (§ 1.2).

Iron(II)-monosulfides can mix in geological terrains with ferromagnesian silicates and their endothermic hydrolyses can proceed in symbiosis with the exothermic alteration of ferromagnesian silicates by water and carbon dioxide. This formation of magnetite at low-T and not at high-T in the serpentinization reaction is to our knowledge not yet reported in the literature, as the hydrothermal formation of magnetite from troilite in the absence of oxygen is not yet reported either.

Table 3 Geological signatures of anoxic and oxic alteration of Fe(II)Mg-silicates and Fe(II)-monosulfides rocks

Type of rocks interacting with water	Minerals formed at 25 °C	Minerals formed at 250–350 °C: geobiotropic minerals
		O ₂ absent in water
Fe(II)Mg-silicates	1. Fe-phyllsilicates Fe ₃ O ₄ at pH 8.5	2. Fe(III)-phyllsilicates at 350 °C, pH > 11.5 Fe(OH) ₃ , FeO(OH), Fe ₂ O ₃ Fe ₃ O ₄ (traces), FeMg-carbonates
Fe(II)-monosulfides	3. FeS ₂	4. Fe ₃ O ₄
		O ₂ present in radiolyzed water
Ferromagnesian silicate	5. Fe ₃ O ₄ Fe(OH) ₃ , FeO(OH), Fe ₂ O ₃	6. Fe ₃ O ₄ Fe(OH) ₃ , FeO(OH), Fe ₂ O ₃
Iron(II) monosulfide	7. FeS ₂ Fe(OH) ₃ , FeO(OH), Fe ₂ O ₃ sulfates	8. Fe ₃ O ₄ Fe(OH) ₃ , FeO(OH), Fe ₂ O ₃ sulfates

When the minerals of Table 3 are produced in hydrothermal conditions, they can lead to the formation of CO and components of life as described in the introduction. In our purpose to determine minerals inside rocks which are signs that prebiotic chemistry occurred at the same location or nearby, we retain the anoxic hydrothermal (350 °C) alteration of ferromagnesian silicate rocks with release of H₂. We also retain the anoxic oxidation of iron(II) monosulfide at elevated temperature (250 °C) with release of H₂. And we retain the oxic oxidation at high-T of ferromagnesian silicate rocks and iron(II)-monosulfide rocks, with release of H₂ from radiolyzed water. These four cases are summarized on the right column of Table 3.

As described in the introduction, synthesis of amino acids following the experiments conducted by K. Kobayashi, requires the presence of CO instead of CO₂. And we reported experiments that produced CO from high temperature hydrogenation of CO₂ (Fu and Seyfried 2009; Chen et al. 2000). Thus in geological terrains, CO forms when hydrogenation of CO₂ may happen in hydrothermal conditions. During asteroidal impacts at the surface of celestial objects, or inside veins, faults, niches, fractures, pores, cavities of rocks and apolar high-pressure high-temperature water, or supercritical water, H₂, CO₂ and N₂ can concentrate (Bassez 1999, 2003): *"The nature of high-pressure water, with its apolar dimers, could be the necessary environmental condition to concentrate the elementary molecules and trigger prebiotic chemistry. Reactions could occur inside cavities acting as chemical reactors or on rock surfaces. Indeed, chimneys are formed from dissolved minerals that precipitate when superhot water meets cold ocean water. It is highly likely that this solid deposition occurring at the turbulent interface between superhot and cold water would create a spongy solid with microcavities and nanochannels of fractal dimensions as well as larger size cavities..."* This scenario that I proposed earlier can apply to different kind of geological sites: meteorites, hydrothermal vents, the surface of the Jupiter's moon Europa and the surface of the Saturn's moon Enceladus, underneath their ocean, and also perhaps Pluto...CO can be produced in hydrothermal conditions and sufficient vapor pressure may be available to initiate prebiotic reactions. Consequently, components of life may form in geological terrains where concentration of H₂, CO₂ and N₂ occurs in hydrothermal conditions and where an excitation source is available. Kobayashi experiments were conducted with 350 Torr CO, 350 Torr N₂ and liquid water producing 20 Torr gaseous water. Following this experiment, the question of the origin of components of life might be reduced to the question: where molecular hydrogen forms in hydrothermal conditions and produce CO in equal amounts of N₂ in the presence of little amount of water and excitation sources? The two anoxic hydrolyses/oxidations of ferromagnesian silicates and iron(II)-monosulfide rocks analyzed respectively at 350 °C and 250 °C, release molecular hydrogen in hydrothermal conditions. They can lead to the synthesis of organic molecules of biological interest, when CO₂ and N₂ are available in the presence of excitation sources and little amount of water. Rocks hydrothermally altered in the absence of oxygen, leave products of alteration which become mineralogical signs of prebiotic chemistry. They are summarized in the cases 2 and 4 of Table 3.

The four oxic hydrolyses/oxidations of ferromagnesian silicates and iron(II) monosulfide rocks at 25 °C and 350–250 °C, do not release H₂. However H₂ is produced and released by radiolyzed water. When hydrothermal conditions are available, for instance during shocks or impacts of extraterrestrial objects, or inside hydrothermal systems, CO can form and also lead to the synthesis of organic molecules of biological interest. When these molecules are blown away and deposited nearby inside shelters, they avoid decomposition by the radiolyzed water which lies beneath the location of their synthesis. Thus rocks hydrothermally altered by the radiolyzed water and the hydrothermal conditions, leave products of alteration which are mineralogical signs of prebiotic chemistry deposited nearby. They are summarized in the cases 6 and 8 of Table 3.

The process of water-rock interaction producing signs of prebiotic chemistry could be named prebiotic mineralogy. This name would include the mineralogy before the emergence of life but does not show precisely that the alteration of minerals is linked to the synthesis of components of life. Thus, I prefer the word geobiotropy to represent the physico-chemical evolution of rocks in association with the formation of molecules of biological interest and I first introduced this term at the LPSC'2016 (Bassez 2016). Geobiotropy is a word constructed with the Greek word ἡ τροπή used by Plato and Aristotle to mean evolution and by R. Clausius (Clausius 1868) in his concept of entropy. Cases 2, 4, 6 and 8 of Table 3 represent geobiotropic signatures which are formed in the process of geobiotropy.

Following the prebiotic synthesis demonstrated in Kobayashi experiments, terrains which can synthesize chains of amino acids must produce H₂ in an hydrothermal environment of CO₂, in the presence of N₂ and either radioactive sources or cosmic radiation. Geobiotropic signatures may be ferric phyllosilicates, ferric trihydroxide, hematite and/or ferric oxide hydroxides including goethite and lepidocrocite, associated with Fe,Mg-carbonates in anoxic ferromagnesian silicate terrains, and magnetite without carbonates in anoxic iron(II) monosulfide terrains, and magnetite, hematite, ferric trihydroxide and/or goethite, lepidocrocite, without carbonates associated or not with sulfates in oxic terrains, as summarized in Table 3. These signatures indicate that H₂ has been produced and that CO may have formed in the heat released by ferromagnesian silicates alteration or impacts. Since hydrothermal conditions are required to form H₂ and CO, the mineral signature pyrite, which appears to be formed at low-T, is not relevant for search of components of life which are synthesized as described above.

Geological Terrains

Mawrth Vallis on Mars

Plausible scenarios are the following. Troilite is proposed to be formed in the primordial nebula (Lauretta et al. 1997; Tachibana and Tsuchiyama 1998; Ciesla 2015). When condensates of the primordial nebula under the form of asteroids and meteorites, fell on objects such as Mars, iron sulfides might be delivered and within the heat of the impact they might transform mainly into magnetite, and also into hematite, ferric trihydroxide, goethite/lepidocrocite and sulfates, following eqs. (15) to (20) of Table 2 and case 8 of Table 3, by the action of the oxygenated water which is radiolyzed by high-LET cosmic radiation. The hydrogen produced in the radiolyzed water escaped above liquid water and produced CO in the hydrothermal conditions of the impact which might have set water in high temperature or supercritical state. Chains of amino acids formed in the presence of N₂, were blown away by the wind and deposited nearby in non-oxidizing areas, where they became sheltered by protective layers and/or inside faults, veins, fractures, cracks. Consequently, components of life may be found in the vicinity of Martian terrains where the geobiotropic signatures mainly magnetite and also hematite, ferric trihydroxide, goethite, lepidocrocite are observed in association with sulfates.

Anoxic oxidation of ferromagnesian silicates can also happen in protected layers, following case 2 of Table 3 and producing Fe(III)-phyllosilicates, iron oxide hydroxides and FeMg-carbonates. This may be the case of Mawrth Vallis. The Mawrth Vallis region on Mars, 22–25°N, 17–21°W shows a general trend of 100–200 m Fe³⁺-rich smectite phyllosilicates and ferric oxide/hydroxide species overlain by a 5–10 m ferrous phase most frequently mixed with the lower Fe³⁺-smectites and sometimes mixed with the upper 10–50 m layers of Al/Si rich unit composed of Al-smectite phyllosilicates, kaolin-group minerals, hydrated amorphous Al/

Si minerals, ferric oxide/hydroxide components and possibly gibbsite and Fe-OH-bearing sulfates such as jarosite. Ferric oxide bearing materials are associated with the lower and upper units. The upper layer is covered with a few-meters thick cap rock (Loizeau et al. 2010; Bishop et al. 2013). The phyllosilicates-rich outcrops are mainly on the west side, around the Oyama crater and there is higher abundance of olivine and pyroxene in the Fe/Mg-phyllosilicate-rich outcrops than in the Al-phyllosilicate-rich outcrops (Gou et al. 2015).

Observation of carbonates is difficult on Mars. Mg-carbonates are detected at Mac Laughlin crater, about 300 km SW of Mawrth Vallis. It may be plausible that carbonates were formed at Mawrth Vallis, but not yet detected. Thus, the Fe(III)-phyllosilicates et Al(III)-phyllosilicates and the ferric oxides hydroxides detected may be the products of anoxic alteration of ferromagnesian silicates rocks as described in case 2 of Table 3. In the upper layer of Mawrth Vallis, Al-clay phyllosilicates are observed. The detailed structure of these phyllosilicates may be of the kind $(Al^{III}, Fe^{III})_2Si_2O_5(OH)_4$ or $(Al^{III}, Fe^{III})_2Si_4O_{10}(OH)_2$ which would be a proof of the hydrolysis and dehydration of Mg-silicates respectively as discussed in §1.1. and consequently a proof of the presence of Mg-silicates and of high exothermic reactions of hydrolysis and carbonation. Thus the upper layer with its Al-clay phyllosilicates and ferric oxide/hydroxide species may be an area of anoxic ferromagnesian silicates alteration (case 2 of Table 3) which was protected by the observed cap rock. In the case where these Mg-silicates were not protected from cosmic radiation, then oxidation of case 6 of Table 3 would have led to magnetite deposits which would be detectable. Thus in the protected upper layer, H_2 has also most probably been released and components of life may have formed when CO_2 and N_2 were available above liquid water in niches, cavities, fractures of the rock. The excitation source may have been cosmic radiation when the synthesis occurred at the limit of the cap rock. If sulfates are present, such as jarosite which is the ferric sulfate $KFe(III)_3(SO_4)_2(OH)_6$, they may be remnants of the oxidic oxidation in radiolyzed water of some iron(II) monosulfide deposited on the surface by meteoritic impact, as shown in §2.3. and cases 7 and 8 of Table 3, or mixed with the ferromagnesian silicates.

In the sublayers of Mawrth Vallis, which are not submitted to cosmic radiation, a radionuclide may act as source of excitation. Fe(III)-phyllosilicates and ferric oxide hydroxides, i.e. goethite/lepidocrocite are detected, thus H_2 has most probably been released following hydrolysis of olivine and pyroxene and case 2 of Table 3. Future detection of radionuclides may evoke the possibility of components of life formation when CO_2 and N_2 were available above liquid water.

Meteorites, Asteroids and Comets

An allusion to precipitation of magnetite from an aqueous solution of ferrous iron has been proposed without explicit demonstration to explain magnetite-sulfide nodules which are overgrown by compositionally pure magnetite in the CV meteorite Mokoia (Brearly and Krot 2013).

Carbonaceous chondrites meteorites contain prebiotic organic matter abiotically synthesized associated with magnetite, for instance, the Tagish Lake meteorite (Herd et al. 2011). Four specimens were analyzed. They are composed of olivine- and pyroxene-bearing chondrules in a porous matrix of phyllosilicates, sulfides, magnetite and carbonates. The total abundances of amino acids decrease in the order 5.6 ppm for 11 h specimen, 0.9 ppm for 5b, 0.04 ppm for 11i and under detection limit for 11v, with an abundance of the nonprotein amino acid α -aminoisobutyric acid in specimen 11 h of 0.2 ppm, while an earlier analysis of D/L- α -ABA reported the value of 84 ppb (Kminek et al. 2002) and another analysis reported a total amount of

amino acids less than 0.1 ppm (Pizzarello et al. 2001). Glycine is the most abundant amino acid in 11 h and upon the isotope value $\delta^{13}\text{C} = +19\text{‰}$ it is suggested to be of extraterrestrial origin. In 11 h, the enantiomeric ratios of alanine, β -amino-*n*-butyric acid and isovaline were racemic, while nonracemic isovaline was detected in 5b, with an L-enantiomeric excess $\sim 7\%$, and no isovaline was identified in 11i. An hydrothermal alteration inside the parent body is proposed. The above reported mineral assemblage can be representative of the anoxic hydrolyses and carbonations of the ferromagnesian silicates associated with the hydrolysis of iron(II) monosulfide, with production of hydrothermal H_2 , as described in Table 1 and eqs. (10) and (11) of Table 2 and in cases 2 and 4 of Table 3. As discussed in §1.1., magnetite may not be the direct product of the hydrolyses of the ferromagnesian silicates, but rather of hydrothermal transformation of iron(II) monosulfide in the absence of oxygen. The production of H_2 in an hydrothermal environment may have formed CO and consecutively amino acids as racemic amino acids were synthesized in laboratory (Kobayashi et al. 1998).

The presence of volatile glycine accompanied by methylamine and ethylamine is reported in the coma of the comet 67P/Churyumov-Gerasimenko: "*Glycine is most probably released from dust grain mantles which heat up in the coma*" and "*mostly correlated to cometary outbursts near perihelion*" (Altwegg et al. 2016). Glycine observations indicate an association with dust particles which "*could contain typical silicates like olivine and pyroxenes, as well as iron sulfides*" (Hilchenbach et al. 2016). Water and carbon dioxide are detected (Migliorini et al. 2016). Molecular nitrogen is also detected but "*the cometary N_2/CO ratio is depleted by a factor of about 25.4 ± 8.9 as compared to the value derived from protosolar N and C abundances*" (Rubin et al. 2015).

Sublimation of glycine has been studied at specific temperatures and pressures (Bassez 1981) and can give information on the conditions for potential hydrolysis of the dust grains. Thus, I plan to study the recent data on 67P/Churyumov-Gerasimenko more in detail.

Hydrothermal Venting Fields

Other terrains may be representative of ferromagnesian silicate and iron(II) monosulfide rocks hydrolyses. For instance I suggest the hydrothermal sites observed on the ocean spreading ridges, such as the active high-temperature Rainbow hydrothermal site which is ultramafic hosted and located at $36^\circ 14\text{ N}$, $33^\circ 54\text{ W}$ on the MAR, Mid-Atlantic Ridge, at a water depth of $\sim 2300\text{ m}$. As the high-temperature vent fields Logatchev ($14^\circ 45\text{ N}$, 2900 m , 360°C) and TAG (26°N , 3650 m , $T = 360^\circ$), Rainbow is located slightly off-axis of the volcanic zone, a few kilometers away from the ridge axis (Mc Caig et al. 2010). Sulfide chimneys vent fluids at $\sim 365^\circ\text{C}$ and pH 2.8, with high Cl (750 mmol.kg^{-1}), Ca (66.6 mmol.kg^{-1}), H_2 (16 mmol.kg^{-1}), CH_4 (2.5 mmol.kg^{-1}), N_2 (1.8 mmol.kg^{-1}), H_2S (1.2 to 1.4 mmol.kg^{-1}), CO ($5\text{ }\mu\text{mol.kg}^{-1}$), 16 to 29 straight chains of saturated hydrocarbons. SO_4 and Mg are absent. (Charlou et al. 2002, 2010). Vent fauna is distributed in areas where vent fluids and seawater mix, at temperature between ca 3°C and 13°C (Desbruyères et al. 2001).

The off-axis Lost City field, located at a water depth $\sim 750\text{ m}$, 15 km W of the MAR axis, at $30^\circ 07\text{ N}$, $42^\circ 07\text{ W}$, vents fluids with near sea water Cl concentrations (542 mmol/kg), Ca (30 mmol.kg^{-1}), H_2 (15 mmol.kg^{-1}), SO_4 (1 to 6 mmol.kg^{-1}), CH_4 (1 – 2 mmol.kg^{-1}), N_2 (0.5 mmol.kg^{-1}), H_2S (0 to 0.22 mmol.kg^{-1}), low molecular weight hydrocarbons, archae, bacteria, macrofaunal communities, calcium carbonate aragonite/brucite chimneys and very poor content of CO_2 and Mg, in a geological setting of serpentine, talc and carbonate veins. Venting temperature rises up to $\sim 90^\circ\text{C}$, pH values are 9 to 12.1 (Kelley et al. 2005; Charlou et al. 2010; Seyfried et al. 2015).

Amino acids are observed inside rocks and fluid samples of the venting fields. They are observed inside two peridotite rock samples which have been dredged on the ocean floor of the Logatchev and Ashadze hydrothermal sites and upon a gas chromatography/mass spectrometry analysis, GCMS, they are inferred to be of biotic origin (Bassez et al. 2009). Dissolved free amino acids are detected in 31 hydrothermal fluid samples of high-T ~ 350 °C and low-T ~ 18 °C venting sites of the MAR, with higher amount than the levels typically found in the deep sea (Klevenz et al. 2010). Amino acids are also detected in the Lost City white vent fluids in greater amount than in seawater and in the plume and it is observed that fluids that are low in hydrogen have higher content of hydrolysable polymers of amino acids (Lang et al. 2013). Amino acids are also detected at other sites than the MAR, for instance polymers of amino acids are detected in the vent fluids (pH ~ 3.3) of the southern Mariana Trough, at 12°55'N, 143°39'E, on an off-axis seamount, and their concentration increase with temperature up to ~ 243 °C (Fuchida et al. 2014).

Both Rainbow and Lost City fields are hosted on ultramafic terrains and vent high amounts of H_2 . However they differ on depth, vent temperature, pH, sulfate content only at Lost City, carbonate chimneys at Lost City and sulfide chimneys at Rainbow. The concentration of H_2S in Lost City is very low, ≤ 0.2 mmol.kg $^{-1}$, compare to the other high T, low pH (3 to 4) vent fields located on the MAR (Ashadze, Logatchev, MARK, TAG, Broken Spur, Rainbow, Lucky Strike and Menez Gwen) where concentrations of H_2S are reported to be between 1.2 and 11 mmol.kg $^{-1}$ (Edmonds 2010; Charlou et al. 2010). Thus the origin of the low- and high-pH fluids seems chemically different. In the next paragraphs, I attempt to understand this difference in pH on a geological basis.

Detachment faults are observed at the high-T, low pH fields Rainbow, Logatchev and TAG. The TAG, Trans-Atlantic Geotraverse field in the rift valley of the MAR, is underlain by hydrothermally altered basaltic rocks. It has been geologically studied in detail. A massive sulfide mound (200 m diameter, 35–50 m high) is surmounted by venting black smokers chimneys. It is populated by a vent ecosystem, mainly shrimps (Mc Caig et al. 2010; Rona 2010). TAG lies on an active hanging wall, or upper layer, of a detachment fault which penetrates until beneath the neovolcanic axis over a depth interval of ~ 3 –7 km below seafloor, with a steep dip (70°) (deMartin et al. 2007). It has been proposed that processes for maintaining TAG long-lived hydrothermal circulation are tectonic rather than volcanic, because of plausible reactivation of the hanging wall permeability due to the fault movements (Tivey et al. 2003). Gabbro and diabase outcrops from the footwall are exposed on the eastern rift valley wall (Fig. 8 of Tivey et al. 2003, Fig. 2 of deMartin et al. 2007). A 125 m drill in the TAG's mound shows that the mound is composed of basalt and four different kind of breccias made of pyrite, calcium sulfate anhydrite, quartz-sulfide and quartz-chlorite, underlain by basalt at depth (Tivey and Dymant 2010).

It is known that gabbro rocks may contain sulfide inclusions. For instance, a recent article discusses the presence of sulfide in rocks which contain the silicates garnet $(Ca,Fe)_3(Al,Cr)_2(SiO_4)_3$ and lawsonite, $CaAl_2Si_2O_7(OH)_2 \cdot H_2O$ (Brown et al. 2014). These minerals may be present in gabbros. I suggest that inside the hanging wall, below the TAG field, hydrothermal fluids may percolate through cracks and fractures of the basalt and gabbro rocks and interact with the ferrous sulfides of the inclusions, producing magnetite and dissolved H_2S at low pH (3.5 to 8 at 250 °C) following eq. (11) of Table 2. Reaction (11) which is endothermic as discussed in §1.2 is deduced from a E-pH diagram at 250 °C. It can proceed within the high-temperature subseafloor fluids and may be at the origin of the low pH 3.1 of the field, the magnetite deposits and the release of H_2S . Consequently, as I proposed earlier (Bassez 2013; Bassez 2016), it may be suggested that it is the hydrolysis/oxidation of ferrous sulfide in the

absence of oxygen (eq. 11) and not the hydrolysis/oxidation of ferromagnesian silicate, which contributes to explain the low pH values 3–4 and the H₂S concentration between 1.2 and 11 mmol/kg, observed at all high-T, low-pH fields. If this suggestion is plausible, magnetite deposits would occur inside the mound below the TAG field, in the hanging wall of the detachment fault, where the fluid percolates hydrothermally. This part of the TAG area should thus be more magnetized. Indeed, magnetic tests conducted on two samples of the mound show the Natural Remnant Magnetization (NRM) typical of basalt (10 A.m⁻¹) and higher magnetic susceptibility with Curie temperatures of 500–540 °C (Tivey and Dymant 2010). Since the Curie temperature of magnetite is 580 °C, I suggest that these magnetic rock analyses of the TAG mound prove the presence of magnetite deposits in the hanging wall and I suggest iron(II) monosulfide such as mackinawite/troilite/pyrrhotite oxidation to be at the origin of these deposits.

The same circulation of fluids through iron sulfide containing rocks may occur at Logatchev and Rainbow. The Logatchev detachment footwall, is composed mainly of ultramafic rocks with gabbroic intrusions (Mc Caig et al. 2010, Fig. 3). At Rainbow, the venting chimneys are composed of iron sulfides. They are of two types, either pyrite FeS₂ /sphalerite ZnFeS/ chalcopyrite CuFeS₂, or pyrrhotite FeS / Fe-sphalerite /chalcopyrite. They emerge from superposed layers of sulfides, mainly pyrite and pyrrhotite, which contain coarse-grained magnetite. The basement layer contains serpentinised peridotite with olivine, pyroxene, serpentine, carbonates veins and dust-like euhedral grains of magnetite (Marques et al. 2006). A magnetic survey of the Rainbow site conducted in 2001 shows a strong positive magnetic anomaly, with magnetization up to 35 A.m⁻¹, on the western side of the field, compared to the 10 A.m⁻¹ in other areas (plate 7 of Tivey and Dymant 2010). Thus the TAG same process of hydrothermal percolation from the detachment fault through deep iron sulfide containing rocks may occur at Rainbow and also at Logatchev.

Consequently, as I propose above, the hydrolysis/oxidation of ferrous monosulfide in the absence of oxygen (eq. 11) may contribute to explain the low pH 3–4 and H₂S concentration (2–11 mmol.kg⁻¹) observed at all high-T, low-pH venting fields and also their local positive magnetic anomalies.

It seems that the high pH Lost City venting fluids would be preferentially represented by the hydrolysis of ferromagnesian silicates. Essential differences in physico-chemical composition, with the high-T, low-pH fields are: very low H₂S concentration, 0 to 0.22 mmol/kg, low fluid temperature, up to 90 °C and high pH, 9–12.1 Hydrolyses in the absence of oxygen, of the iron silicates fayalite and ferrosilite, following eq. (10) deduced from E-pH diagrams, lead to high pH ~11.5 to 14 at 350 °C. Lost City would thus rely more on serpentinization processes with cooling of the uplifted fluids. However, Lost City fluids contain SO₄ which is usually produced through oxidation of H₂S by oxygen. This dilemma about the presence of oxygen may be solved considering oxidation by oxygen produced in water which would be locally ionized. Since the S-isotope composition of sulfate ($\delta^{34}\text{S}$) at Lost City reaches the troilite value of the Canyon Diablo meteorite, it may perhaps be suggested that sulfate is synthesized at T ~ 150–250 °C following eqs. (15) to (19) of Table 2, from some occasional troilite available in deep seafloor near a radioactive source emitting high energy α -particles which locally ionize water and produce oxygen. Several radioactive hotspots are known on Earth. For instance, the Paralana hot spring, located near Arkaroola in the Northern Flinders Ranges, South Australia, shows uplifted uranium-rich granites and contains water at pH 7 and 60–63 °C, bubbling gas with radon, an alpha-particles emitter and microbial mats. At Paralana, water is believed to be heated by geothermal processes and radioactive decay (Anitori and Henneberger 2004). Even if Lost City is mainly serpentinization driven, an alpha-particles

radioactive source is not excluded to be a local supply of oxygen and formation of SO_4 . As discussed in § 2.1, O_2 is produced only if water is ionized by high energy particles.

Radioactive sources are most probably present inside rocks on the mid-atlantic ridge. Potassium may be present in clays and only with a very low content in ultramafic rocks. However, thorium and uranium are present as trace elements in most silicate rocks (Supper et al. 2013). They are incorporated for instance as Th^{4+} and U^{4+} in thorite $\text{Th}(\text{SiO}_4)$, huttonite $(\text{Th},\text{U})(\text{SiO}_4)$, coffinite $\text{U}[\text{SiO}_4(\text{OH})_4]$ and cheralite $[\text{Ce},\text{Ca},\text{Th},\text{U}](\text{P},\text{Si})\text{O}_4$, with U replacing sometimes Th. Huttonite and cheralite are within the structure group of monazite $[(\text{REE})\text{PO}_4]$ (Hazen et al. 2009). REE is for Rare Earth Elements. Pleochroic halos are known around radioactive monazite inclusions inside biotite (IAEA 2003). They are caused by the high-energy alpha-particles ${}^4\text{He}^{2+}$ emitted by ${}^{232}\text{Th}$ and ${}^{238}\text{U}$ decay radionuclides, and they are commonly observed in the phosphates monazite, xenotime (YPO_4) and apatite $\text{Ca}_5(\text{PO}_4)(\text{OH},\text{F},\text{Cl})$ and in the silicates biotite, amphiboles and zircon. Biotite is a phyllosilicate of the mica group $\text{K}(\text{Mg},\text{Fe}^{2+})_3[\text{AlSi}_3\text{O}_{10}(\text{OH},\text{F})_2]$, amphibole is a group of double chain inosilicates $(\text{Mg},\text{Fe})_7\text{Si}_8\text{O}_{22}(\text{OH})_{22}$, and zircon a group of neosilicate ZrSiO_4 . Biotite is found for instance in the ultramafic alkaline rock biotite peridotite-porphyrite of the Siberian Aldan shield, which consists of olivine, pyroxene and biotite (Chepurov 1974). Recent experiments show radiohaloes surrounding the 1.8 Ga old Th-rich inclusions of monazite $(\text{Ce}_{0.40}\text{La}_{0.22}\text{Nd}_{0.12}\text{Pr}_{0.04}\text{Sm}_{0.03}\text{Th}_{0.15}\text{U}_{0.02}\text{Si}_{0.02})\text{PO}_4$, in the TOT sheet silicate biotite. Alpha-particles in the ${}^{232}\text{Th}$ and ${}^{238}\text{U}$ decay chains leave their source with an initial energy of 4–8 MeV depending on the parent isotope and cause damage, reducing a homogenous laterally continuous crystal into discrete domains of expansion and contraction and even amorphization. Alpha-particles do not penetrate deeply and their effect stays around the inclusion, creating crystal distortion (Bower et al. 2016). Thus any kind of alpha-emitter can produce local water ionization and formation of O_2 in the proximate circulating hydrothermal fluids. Water locally radiolyzed can induce specific chemical synthesis as I proposed earlier (Bassez 2003, 2008, 2009a, 2009b). For instance, water, CO_2 and N_2 may have been captured in micro and nanopores located inside rocks, nearby a radionuclide alpha emitter. Their concentration in the gas phase above the liquid pore water, may be sufficient to start a prebiotic synthesis and produce amino acids, following Kobayashi experiments. After an indeterminate number of years, these rocks may fracture, thus triggering more complex reactions.

We have thus attempted to explain the differences in temperature and pH values of the high-T and low-T vents by considering the geological and magnetic environment coupled to thermodynamic functions calculations for the elementary reactions of the serpentinization process and to redox equations extracted from thermodynamic E-pH diagrams. We propose that the endothermic mackinawite/troilite/pyrrhotite oxidation can proceed in symbiosis with the exothermic serpentinization reactions of the ultramafic hosted low-pH hydrothermal vents of the spreading ridges, and that it can contribute to explain the low pH values, the H_2S concentrations and the local positive magnetic anomalies. The process of water locally radiolyzed is suggested to explain formation of sulfate at the high pH Lost City vent.

Conclusion

In this article, the results and the drawn tables are based on calculations of thermodynamics functions and analyses of published E-pH diagrams. Four E-pH diagrams which were drawn for corrosion purposes are analyzed: (Fig.7a p. 329 of Cook and Olive 2012, Fig.4 p. 312

of Pourbaix 1963, Fig.1 and Fig.2 of Macdonald 1992). They are assembled in: (Bassez 2017a and Bassez 2017b).

The results show that the anoxic hydrothermal hydrolysis/oxidation of iron(II)-monosulfides leads to pyrite and H₂ at 25 °C and to magnetite and H₂ at 250 °C, and that this last endothermic reaction may occur within the heat produced by the hydrolyses and carbonations of ferromagnesian silicate rocks. It is suggested that this FeS anoxic oxidation may also happen within magmatic or impact heat. Upon the results of our analyses which are confirmed by various laboratory experiments, it is shown that the anoxic hydrolysis of ferrous silicates leads mainly to Fe(III)-phyllosilicates, ferric trihydroxide, goethite, lepidocrocite, hematite and FeMg-carbonates. Magnetite is a secondary product. It can be produced when iron(II)-monosulfides are mixed with ferromagnesian silicates. Molecular hydrogen is thus produced in the serpentinization process during anoxic hydrolysis/oxidation of ferrous ion not into magnetite, but into ferric trihydroxide, goethite, lepidocrocite, hematite and Fe(III)-phyllosilicates, and also during anoxic hydrolysis/oxidation of iron(II)-monosulfides into magnetite. The case of radiolyzed water is discussed. When ferromagnesian silicates are hydrolyzed/oxidized at 25 °C and at 350 °C, in oxygenated water, magnetite, hematite, ferric trihydroxide, goethite and lepidocrocite are formed. Oxidation of iron(II)-monosulfides at 25 °C leads mainly to pyrite associated to hematite, ferric trihydroxide, goethite/lepidocrocite and sulfates, and at 250 °C mainly to magnetite instead of pyrite, associated to the same ferric oxide/hydroxides and sulfates.

The anoxic hydrolysis of ferromagnesian silicate is proposed to explain the Fe(III)- and Al(III)-phyllosilicates and the ferric oxide hydroxides observed at Mawrth Vallis on Mars. The author shows the importance of the anoxic ferrous sulfide hydrolysis in objects which fell on Earth such as the Tagish Lake meteorite in an attempt to explain their content and witnessed effects. This reaction is also evoked to understand hydrothermal vents with low-pH, high-T, high H₂S contents and magnetic anomalies. The case of the comet 67P/Churyumov-Gerasimenko is planned to be reported later.

As earlier, Marie Paule Bassez proposes that components of life may form as a result of water rock interaction when hydrogen is released hydrothermally, in the presence of CO₂, N₂ and an excitation source such as those used to obtain prebiotic molecules from mixtures of CO, N₂ and H₂O. The cases of H₂ produced during ferromagnesian silicates and iron(II)-monosulfides hydrolyses and during water radiolysis are discussed. M P Bassez proposes a name, the geobiotropic signatures, for the minerals which witness this plausible formation of components of life during the process of geobiotropy, the evolution from rock to life.

Acknowledgements Marie Paule Bassez expresses her gratitude to William Cook, University of New-Brunswick, Canada and Digby Macdonald, Pennsylvania State University, USA, for giving permission to analyze with the purpose of prebiotic chemistry, the E-pH diagrams they drew for corrosion purposes. M P Bassez thanks also warmly Michel Cassir and Kevin Ogle, Ecole Nationale Supérieure de Chimie de Paris, France, for fertile discussions on E-pH diagrams and Richard Welter, Université de Strasbourg, France, for positive inputs on redox equations analyses. M P Bassez is also grateful to the reviewer for useful comments.

References

- Aaberg I, Dideriksen K, Rodriguez-Blanco DJ, Regnarsson E, Olsson J, Jespersen TH, Schaumburg K, Stipp SLS (2013) Carbonation of olivine at CO₂ supercritical conditions: Reactivity differences between synthetic and natural olivines. *Goldschmidt* 2013; P216. <http://goldschmidt.info/2013/abstracts/finalPDFs/551.pdf>

- Albarède F (2003) *Geochemistry*. Cambridge University Press, New-York
- Altwegg K, Balsiger H, Bar-Nun A, Berthelier JJ et al (2016) Prebiotic chemicals—amino acid and phosphorus—in the coma of comet 67P/Churyumov-Gerasimenko. *Sci Adv* 2(5):e1600285
- Anitori PR, Henneberger MR (2004) A radon resistant microbial community. *Microbiol-Au* 25(1):30–32
- Aubourg C, Pozzi JP (2010) Toward a new <250°C pyrrhotite-magnetite geothermometer for claystones. *Earth Planet Sc Lett* 294:47–57
- Baldacchino G, Hickel B (2008) Water radiolysis under extreme conditions. Application to the nuclear industry. In: Spothem-Maurizot M, Mostafavi M, Douki T, Belloni J (eds) *Radiation chemistry: from basics to applications in material and life sciences* EDP Sciences
- Bassez MP (1981) Etude spectrochimique de la glycine et de quelques molécules connexes. Analyse rotationnelle et observations du milieu interstellaire. Thesis/Docteur d'Etat-Université de Paris-Sud-Orsay, October 12th, N° 2498
- Bassez MP (1998–2013) La Chimie-Physique en ligne: Thermodynamique et Cinétique Chimiques, Université de Strasbourg. <http://chemphys.u-strasbg.fr/mpb/teach/coursenligne.html> and e-book in preparation
- Bassez MP (1999) La structure de l'eau supercritique et l'origine de la vie. In: *Sciences et technologies: regards croisés en sciences pour l'ingénieur, informatique, mathématiques, biologie, biochimie, chimie*. L'Harmattan ed ISBN 2–7384–7367-9, p. 583–591
- Bassez MP (2003) Is high-pressure water the cradle of life? *J Phys-Condens Mat* 15:L353–L361
- Bassez MP (2008) Synthèse prébiotique dans les conditions hydrothermales. *Proc CNRIUT2008:Lyon* <http://iris.cnrs.fr/~cnriut08/actes/> access 29May/C
- Bassez MP (2009a) Synthèse prébiotique dans les conditions hydrothermales. *CR Chim* 12(6–7):801–807
- Bassez MP (2009b) Prebiotic synthesis under hydrothermal conditions. *Proc ISSOL2008:Firenze. Origins Life Evol B* 39(3–4):223–225
- Bassez MP (2013) Geochemical origin of biological molecules. *EGU2013:Vienna, At, Geophys Res Abstr* 15: EGU2013–22, Oral PS8.1/9:30. <http://meetingorganizer.copernicus.org/EGU2013/EGU2013-22.pdf>
- Bassez MP (2014) Ferromagnesian rocks in association with carbonates as signature for life. *EANA2014: Edinburgh, Uk, Oral-Oct13th*
- Bassez MP (2015) Water, air, earth and cosmic radiation. *Proc ORIGINS2014:Nara, Jp. Origins Life Evol B* 45(1):5–13
- Bassez MP (2016) *Geobiology. LPSC2016:The Woodlands, USA; Abstr #1853*. <http://www.hou.usra.edu/meetings/lpsc2016/pdf/1853.pdf>
- Bassez MP (2017a) Géobiologie, Université de Strasbourg. <http://chemphys.u-strasbg.fr/mpb/teach/originevie/Geobiologie.pdf> and e-book 2017 “Chemphys”
- Bassez MP (2017b) *Geobiology and martian meteorites* http://www.mdpi.com/journal/geosciences/special_issues/martian_meteorites
- Bassez MP, Takano Y, Ohkouchi N (2009) Organic analysis of peridotite rocks from the Ashadze and Logatchev hydrothermal sites. *Int J Mol Sci* 10:2986–2998
- Bassez MP, Takano Y, Kobayashi K (2012) Prebiotic organic microstructures. *Origins Life Evol B* 42:307–316
- Bina M, Coppel J, Daly L, Debeglia N (1991) Transformation de la pyrrhotite en magnétite sous l'effet de la température: une source potentielle d'anomalies magnétiques. *C.R. Acad. Sci. Paris* 313, Série II: 487–494
- Bishop LJ, Loizeau D, McKeown KN, Saper L, Dyar MD, Des Marais JD, Parente M, Murchie LS (2013) What the ancient phyllosilicates at Mawrth Vallis can tell us about possible habitability on early Mars. *Planet Space Sci* 86:130–149
- Bower RW, Patrick ADR, Pearce IC, Droop TRG, Haigh JS (2016) Radiation damage haloes in biotite investigated using high-resolution transmission electron microscopy. *Am Mineral* 101:105–110
- Brearily JA, Krot NA (2013) Metasomatism in the early solar system: the record from chondritic meteorites. In: D.E. Harlov & H Austrheim (ed.) *Metasomatism and the chemical transformation of rock. The role of fluids in terrestrial and extraterrestrial processes*. Springer p688
- Brown LJ, Christy GA, Ellis JD, Arculus JR (2014) Prograde sulfide metamorphism in blueschist and eclogite, New Caledonia. *J Petrol* 55(3):643–670
- Bullock ES, Gounelle M, Lauretta SD, Grady MM, Russell SS (2005) Mineralogy and texture of Fe-Ni sulfides in CI1 chondrites. *Geochim Cosmochim Acta* 69(10):2687–2700
- Buxton VG (2008) An overview of the radiation chemistry of liquids. In: Spothem-Maurizot M, Mostafavi M, Douki T, Belloni J (eds) *Radiation chemistry: from basics to applications in material and life sciences* EDP Sciences
- Charlou JL, Donval JP, Fouquet Y, Jean-Baptiste P, Holm N (2002) Geochemistry of high H₂ and CH₄ vent fluids issuing from ultramafic rocks at the rainbow hydrothermal field. *Chem Geol* 191:345–359
- Charlou JL, Donval JP, Konn C, Ondréas H, Fouquet Y (2010) High production and fluxes of H₂ and CH₄ and evidence of abiotic hydrocarbon synthesis by serpentinization in ultramafic-hosted hydrothermal systems on the Mid-Atlantic Ridge, table 1. In: Rona AP, Devey WC, Dymant J, Murton JB (ed) *Diversity of hydrothermal systems on slow spreading ocean ridges*. AGU:Washington DC, *Geophys Monograph* 188

- Chen CS, Cheng WH, Lin SS (2000) Mechanism of CO formation in reverse water-gas shift reaction over Cu/Al₂O₃ catalyst. *Catal Lett* 68:45–48
- Chepurou IA (1974) Crystallization temperature of biotite peridotite-porphyrite from Central Aldan region. *Int Geol Rev* 16(3):359–360
- Chirita P, Descotes M, Schlegel ML (2008) Oxydation of FeS by oxygen-bearing acidic solutions. *J Colloid Interf Sci* 321:84–95
- Chivot J (2004) Thermodynamique des produits de corrosion. Fonctions thermodynamiques, diagrammes de solubilité, diagrammes E-pH des systèmes Fe-H₂O, Fe-CO₂-H₂O, Fe-S-H₂O, Cr-H₂O et Ni-H₂O en fonction de la température. ANDRA Coll Sc et Tech/CEA:Paris. www.andra.fr
- Christensen AN (1968) Hydrothermal preparation of goethite and hematite from amorphous iron(III) hydroxide. *Acta Chem Scand* 22:1487
- Ciesla JF (2015) Sulfurization of iron in the dynamic solar nebula and implications for planetary compositions. *Astrophys J Lett* 800:L6
- Clausius R (1868) *Théorie Mécanique de la Chaleur*, Jacques Gabay (ed) Paris:1991, Folie F (trad) p.411
- Cook GW, Olive PR (2012) Pourbaix diagrams for the iron-water system extended to high & low-supercritical conditions. *Corros Sci* 55:326–331
- Crumièrre F, Vandendorre J, Essehli R, Blain G, Barbet J, Fattahi M (2013) LET effects on the hydrogen production induced by the radiolysis of pure water. *Radiat Phys Chem* 82:74–79
- Daniels M, Wigg E (1966) Oxygen as a primary species in radiolysis of water. *Science* 153:1533–1534
- Dekkers MJ (1990) Magnetic properties of natural goethite: III magnetic behaviour and properties of minerals originating from goethite dehydration during thermal demagnetization. *Geoph J Int* 103:233–250
- Desbruyères D, Biscoito M, Caprais JC, Colaço A, Comtet T, Crassous P, Fouquet Y, Khripounoff A, Le Bris N, Olu K, Riso R, Sarradin PM, Segonzac M, Vangriesheim A (2001) Variations in deep-sea hydrothermal vent communities on the mid-Atlantic ridge near the Azores plateau. *Deep-Sea Res I* 48:1325–1346
- Dos Santos CE, de Mendoça Silva CJ, Duarte AH (2016) Pyrite oxidation mechanism by oxygen in aqueous medium. *J Phys Chem C* 120:2760–2768
- Edmonds NH (2010) Chemical signatures from hydrothermal venting on slow spreading ridges, table 3. In: Rona AP, Devey WC, Dymont J, Murton JB (ed) Diversity of hydrothermal systems on slow spreading ocean ridges. AGU:Washington DC, *Geophys Monograph* 188
- Ferradini C, Jay-Gerin JP (1999) La radiolyse de l'eau et des solutions aqueuses: historique et actualité. *Can J Chemistry* 77:1542–1575
- Fu Q, Seyfried Jr EW (2009) Experimental study of abiotic synthesis processes in a hydrothermal flow system. *LPS2009: The Woodlands; Abstr #2504*
- Fuchida S, Mizuno Y, Masuda H, Toki T, Makita H (2014) Concentrations and distributions of amino acids in black and white smoker fluids at temperatures over 200°C. *Org Geochem* 66:98–106
- Gervais B, Beuve M, Olivera HG, Galassi EM, Rivarola DR (2005) Production of HO₂ and O₂ by multiple ionization in water radiolysis by swift carbon ions. *Chem Phys Lett* 410:330–334
- Gou S, Yue Z, Di K, Wang J (2015) Mineral abundances and different levels of alteration around Mawrth Vallis, Mars. *Geosci Frontiers* 6:741–758
- Gualtieri FA, Venturelli P (1999) In situ study of the goethite-hematite phase transformation by real time synchrotron powder diffraction. *Am Mineral* 84:895–904
- Hazen MR, Ewing CR, Sverjensky AD (2009) Evolution of uranium and thorium minerals. *Am Mineral* 94:1293–1311
- Herd DKC, Blinova A, Simkus ND, Huang Y, Tarozo R, MO'DC A, Gyngard F, Nittler RL, Cody DG, Fogel LM, Kebukawa Y, ALD K, Hilts WR, Slater FG, Glavin PD, Dworkin PJ, Callahan PM, Elsila EJ, De Gregorio TB, Stroud MR (2011) Origin and evolution of organic matter as inferred from the Tagish Lake meteorite. *Science* 332:1304
- Hilchenbach M, Kissel J, Langevin Y, Briois C et al (2016) Comet 67P/Churyumov-Gerasimenko: close-up on dust particle fragments. *Ap J Lett* 816:L32
- Huang PY, Leung L, Novotny R, Sedov A, Matsui H (2016) Supercritical water-cooled reactor. 10th GIF-INPRO/IAEA Interface meeting-Vienna, April 11–12
- IAEA (2003) Guidelines for radioelement mapping using gamma ray spectrometry data. *Int Atom Energy Agency: Vienne, IAEA-TECDOC-1363* p.122
- Jones FC, LeCount S, Smart SCR, White JT (1992) Compositional and structural alteration of pyrrhotite surfaces in solution: XPS and XRD studies. *Appl Surf Sci* 55:65–85
- Kars M, Aubourg C, Pozzi JP, Janots D (2012) Continuous production of nanosized through low grade burial. *Geochem Geophys Geosy* 13(8):1–12
- Kelley SD, Karson AJ, Frühn-Green GL, Yoerger RD, Shank MT et al (2005) A serpentinite-hosted ecosystem: the lost City hydrothermal field. *Science* 307:1428

- Klein F, Grozeva GN, Seewald SJ, McCollom MT, Humphris ES, Moskowitz B, Berquo ST, Kahl WA (2015) Experimental constraints on fluid-rock reactions during incipient serpentinization of harzburgite. *Am Mineral* 100:991–1002
- Klevenz V, Sumoondur A, Ostertag-Henning C, Koschinsky A (2010) Concentrations and distributions of dissolved amino acids in fluids from mid-Atlantic ridge hydrothermal vents. *Geochem J* 44:387–397
- Kminek G, Botta O, Glavin PD, Bada LJ (2002) Amino acids in the Tagish Lake meteorite. *Meteorit Planet Sci* 37:697–701
- Kobayashi K, Tsuchiya M, Oshima T, Yanagawa H (1990) Abiotic synthesis of amino acids and imidazole by proton irradiation of simulated primitive earth atmospheres. *Origins Life Evol B* 20:99–109
- Kobayashi K, Kaneko T, Saito T, Oshima T (1998) Amino acid formation in gas mixtures by high energy particle irradiation. *Origins Life Evol B* 28:155–165
- Kobayashi K, Ogawa T, Tonishi H, Kaneko T, Takano Y, Takahashi JI, Saito T, Muramatsu Y, Yoshida S, Utsumi Y (2008) Synthesis of amino acid precursors from simulated interstellar media by high-energy particles or photons. *Electron Commun Japan* 91(3):15–21
- Lang SQ, Früh-Green GL, Bernasconi SM, Butterfield DA (2013) Sources of organic nitrogen at the serpentinite-hosted Lost City hydrothermal field. *Geobiology* 11(2):154–169
- Lauretta SD, Lodders K, Fegley B Jr (1997) Experimental simulations of sulfide formation in the solar nebula. *Science* 277:358
- Le Caër S (2011) Water radiolysis: influence of oxide surfaces on H₂ production under ionizing radiation. *Water* 3:235–253 www.mdpi.com/journal/water
- Lennie RA, Redfern ATS, Champness EP, Stoddart PC, Schofield FP, Vaughan JD (1997) Transformation of mackinawite to greigite: an in situ X-ray powder diffraction and transmission electron microscope study. *Am Mineral* 82:302–309
- Li W, Beard LB, Li C, Johnson MC (2014) Magnesium isotope fractionation between brucite Mg(OH)₂ and Mg aqueous species: implications for silicate weathering and biogeochemical processes. *Earth Planet Sc Lett* 394:82–93
- Liedhegner EJ, Jennings W, Wainright J (2011) Rapid electrochemical detection of radiolysis products in an aqueous solution exposed to alpha particle beams. *Int J Electrochem* 2011:864126
- Lin M, Muroya Y, Baldacchino G, Katsumura Y (2010) Radiolysis in supercritical water. In: Wishart FJ, Rao BSM (eds) *Recent trends in radiation chemistry*. World Scientific Publ
- Loizeau D, Mangold N, Poulet F, Ansan V, Hauber E, Bibring JP, Gondet B, Langevin Y, Masson P, Neukum G (2010) Stratigraphy in the Mawrth Vallis region through OMEGA, HRSC color imagery and DTM. *Icarus* 205:396–418
- Lovering FJ, Parry GL (1962) Thermomagnetic analysis of co-existing nickel-iron metal phases in iron meteorites and the thermal histories of the meteorites. *Geochim Cosmochim* 26:361–382
- Macdonald DD (1992) Critical issues in the use of metals and alloys in sulphur-containing aqueous systems. Annual conference of metallurgists on materials performance, sulphur and energy, Edmonton, Ca, 24–27 August, <https://www.osti.gov/scitech/biblio/6395030>. OSTI 1993 report n° 6395030 <https://www.osti.gov/scitech/servlets/purl/6395030>
- Marques AFA, Barriga JASF, Chavagnac V, Fouquet Y (2006) Mineralogy, geochemistry and Nd isotope composition of the rainbow hydrothermal field, mid-Atlantic ridge. *Mineral Deposita* 41(1):52–67
- deMartin JB, Sohn AR, Canales PJ, Humphris ES (2007) Kinematics and geometry of active detachment faulting beneath the trans-Atlantic Geotraverse (TAG) hydrothermal field on the mid-Atlantic ridge. *Geology* 35(8): 711–714
- Mc Caig MA, Delacour A, Fallick EA, Castelain T, Früh-Green LG (2010) Detachment fault control on hydrothermal circulation systems: interpreting the subsurface beneath the TAG hydrothermal field using the isotopic and geological evolution of oceanic core complexes in the Atlantic. In: Rona AP, Devey WC, Dymont J, Murton JB (ed) *Diversity of hydrothermal systems on slow spreading ocean ridges*. AGU: Washington DC, *Geophys Monograph* 188
- Migliorini A, Piccioni G, Capaccioni F, Filacchione G, Bockelée-Morvan D, Erard S, Leyrat C, Combi RM, Fougere N, Crovisier J, Taylor WF, De Sanctis CM, Capria TM, Grassi D, Rinaldi G, Tozzi PG, Fink U (2016) Water and carbon dioxide distribution in the 67P/Churyumov-Gerasimenko coma from VIRTIS-M infrared observations. *Astron Astrophys* 589:A45. doi:10.1051/0004-6361/201527661
- Monazam RE, Breault WR, Siriwardane R (2014) Kinetics of magnetite (Fe₃O₄) oxidation to hematite (Fe₂O₃) in air for chemical looping combustion. *Ind Eng Chem Res* 53(34):13320
- Özdemir Ö, Dunlop JD (2000) Intermediate magnetite formation during dehydration of goethite. *Earth Planet Sc Lett* 177:59–67
- Pizzarello S, Huang Y, Becker L, Poreda JR, Nieman AR, Cooper G, Williams M (2001) The organic content of the Tagish Lake meteorite. *Science* 293:2236–2239

- Popova PO, Jennikens P, Emel'yanenko V, Kartashova A, Biryukov E et al (2013) Chelyabinsk airburst, damage assessment, meteorite recovery, and characterization. *Science* 342:1069–1073
- Pourbaix M (1963) Atlas d'équilibres électrochimiques. Gauthier-Villars (ed): Paris
- Rickard D (1997) Kinetics of pyrite formation by the H₂S oxidation of iron (II) monosulfide in aqueous solutions between 25 and 125°C: the rate equation. *Geochim Cosmochim* 61(1):115
- Rinaudo C, Gastaldi D, Belluso E (2003) Characterization of chrysotile, antigorite and lizardite by FT-Raman spectroscopy. *Can Mineral* 41:883–890
- Robie RA, Hemingway BS (1995) Thermodynamic properties of minerals at 298.15K and 1 bar (10⁵ Pa). US Geological Survey Bull 2131
- Rona AP (2010) Emerging diversity of hydrothermal systems on slow spreading ocean ridges, §5. In: Rona AP, Devey WC, Dymont J, Murton JB (ed) Diversity of hydrothermal systems on slow spreading ocean ridges. AGU:Washington DC, *Geophys Monograph* 188
- Rubin M, Altwegg K, Balsiger H, Bar-Nun A et al (2015) Molecular nitrogen in comet 67P/Churyumov-Gerasimenko indicates a low formation temperature. *Science* 348(6231):323–235
- Sanguanmith S, Meesungnoen J, Jay-Gerin JP (2012) Density dependence of the "escape" yield of hydrated electrons in the low-LET radiolysis of supercritical water at 400°C. *Phys Chem Chem Phys* 14(32):11277
- Santos-Carballal D, Roldan A, de Leeuw HN (2016) Early oxidation processes on the greigite Fe₃S₄(001) surface by water: a density functional theory study. *J Phys Chem C* 120:8616–8629
- Schlesinger G, Miller LS (1983) Prebiotic synthesis in atmospheres containing CH₄, CO, and CO₂. *J Mol Evol* 19:376–382
- Seyfried EW Jr, Foustoukos DI, Fu Q (2007) Redox evolution and mass transfer during serpentinization. *Geochim Cosmochim Acta* 71:3872–3886
- Seyfried EW Jr, Pester JN, Tutolo MB, Ding K (2015) The lost city hydrothermal system: constraints imposed by vent fluid chemistry and reaction path models on subseafloor heat and mass transfer processes. *Geochim Cosmochim Acta* 163:59–79
- Supper R, Baron I, Ottowitz D, Motschka K, Gruber S, Winkler E, Jochum B, Römer A (2013) Airborne geophysical mapping as an innovative methodology for landslide investigation: evaluation of results from the Gschliefgraben landslide, Austria. *Nat Hazard Earth Sys* 13:3313–3328
- Tachibana S, Tsuchiyama A (1998) Incongruent evaporation of troilite in the primordial solar nebula: an experimental study. *Geochim Cosmochim Acta* 62(11):2005–2022
- Tivey AM, Dymont J (2010) The magnetic signature of hydrothermal systems in slow spreading environments. In: Rona AP, Devey WC, Dymont J, Murton JB (ed) Diversity of hydrothermal systems on slow spreading ocean ridges. AGU:Washington DC, *Geophys Monograph* 188
- Tivey AM, Schouten H, Kleinrock MC (2003) A near-bottom magnetic survey of the mid-Atlantic ridge axis at 26°N: implications for the tectonic evolution of the TAG segment. *J Geophys Res* 108(5):2277
- Usher RC, Cleveland AC Jr, Strongin RD, Schoonen AM (2004) Origin of oxygen in sulfate during pyrite oxidation with water and dissolved oxygen: an in-situ horizontal attenuated total reflectance infrared spectroscopy isotope study. *Environ Sci Technol* 38:5604–5606